Purkinje cell neurotransmission patterns cerebellar basket cells into zonal modules that are defined by distinct pinceau sizes

Joy Zhou[1,2,4,*], Amanda M. Brown[1,2,4,*], Elizabeth P. Lackey[1,2,4], Marife Arancillo[1,4], Tao Lin[1,4], Roy V. Sillitoe[1,2,3,4]

[1]Department of Pathology & Immunology, [2]Department of Neuroscience, [3]Program in Developmental Biology, Baylor College of Medicine, [4]Jan and Dan Duncan Neurological Research Institute of Texas Children's Hospital, 1250 Moursund Street, Suite 1325, Houston, Texas 77030, USA

Address correspondence to Dr. Roy V. Sillitoe

*These authors contributed equally

Tel: 832-824-8913
Fax: 832-825-1251
Email: sillitoe@bcm.edu

Manuscript contains:

Number of pages: 52
Number of figures: 9 Figures, 3 Figure Supplements
Number of words: Abstract (148**)**

Abbreviated title: Diversity of cerebellar basket cell projections

Keywords: cerebellum, interneuron, pinceaux, inhibition, circuitry, patterning, zebrinII

Contributions: JZ, AMB, MA and RVS designed the experiments. JZ, AMB, EPL, MA, TL and RVS performed the experiments. JZ, AMB and RVS wrote and edited the paper.

Competing Interests: We do not have any competing interests and have nothing to disclose.

Acknowledgements
This work was supported by funds from Baylor College of Medicine (BCM) and Texas Children's Hospital. RVS received support from The Bachmann-Strauss Dystonia and Parkinson Foundation, Inc., The Caroline Wiess Law Fund for Research in Molecular Medicine, The Hamill Foundation, BCM IDDRC U54HD083092, National Center for Research Resources C06RR029965, and the National Institutes of Neurological Disorders and Stroke (NINDS) R01NS089664 and R01NS100874. The BCM IDDRC Neuropathology Core performed the immunohistochemistry and histology experiments. The content is solely the responsibility of the authors and does not necessarily represent the official views of the National Center for Research Resources or the National Institutes of Health. AMB received support from F31NS101891 and MA was supported by a postdoctoral award from the National Ataxia Foundation (NAF).

Abstract

Ramón y Cajal proclaimed the neuron doctrine based on circuit features he exemplified using cerebellar basket cell projections. Basket cells form dense inhibitory plexuses that wrap Purkinje cell somata and terminate as pinceaux at the initial segment of axons. Here, we demonstrate that HCN1, Kv1.1, PSD95 and GAD67 unexpectedly mark patterns of basket cell pinceaux that map onto Purkinje cell functional zones. Using cell-specific genetic tracing with an *Ascl1*^{CreERT2} mouse conditional allele, we reveal that basket cell zones comprise different sizes of pinceaux. We tested whether Purkinje cells instruct the assembly of inhibitory projections into zones, as they do for excitatory afferents. Genetically silencing Purkinje cell neurotransmission blocks the formation of sharp Purkinje cell zones and disrupts excitatory axon patterning. The distribution of pinceaux into size-specific zones is eliminated without Purkinje cell output. Our data uncover the cellular and molecular diversity of a foundational synapse that revolutionized neuroscience.

Introduction

Studies of the cerebellar basket cell, first by Camillo Golgi and then by Santiago Ramón y Cajal, hold a special place in history. In particular, it was Cajal's discovery that the endings of basket cells terminate upon what would become known as the initial segment of the Purkinje cells that sparked a new era of neuroscience (Cajal, 1911). He called this nerve ending "the pinceau", named for its paintbrush-like appearance. Anatomical analyses revealed the complexity of this synapse as a dense and intriguing set of contacts that played a key role in the debate of whether neurons were individual units connected by synapses or whether they were unified in a reticulum with a somewhat uninterrupted flow of information. The complexity of the basket cell pinceau hid its true connectivity when studied using the Golgi reaction, although using electron microscopy, Sanford Palay and Victoria Chan-Palay resolved the full architecture of the basket cell axons, their collaterals, the pericellular baskets that wrap around the Purkinje cell soma, and the pinceau terminals that contact the initial segment of the Purkinje cell axon (Palay and Chan-Palay, 1974). The surprising sparseness of synaptic contacts between the pinceau and the Purkinje cell axon (Palay and Chan-Palay, 1974; Somogyi and Hamori, 1976)–although reliably found on the Purkinje cell axons of different species (Hamori and Szentagothai, 1965)–was, at the time, consistent with the relatively weak functional inhibitory connectivity shown by slice electrophysiology recordings (Eccles et al., 1967; Korn and Axelrad, 1980). More than three decades later, advanced slice electrophysiology recording methods revealed an unexpected ultra-fast ephaptic mode of axon-to-axon communication between basket cells and Purkinje cells (Blot and Barbour, 2014). Accordingly, the collective repertoire of contacts between the two cell types makes a substantial functional contribution, as genetic silencing of GABAergic basket cell output alters Purkinje cell firing *in vivo* (Brown et al., 2019). There is also evidence showing that

basket cells play an essential role in controlling cerebellar cortical output during motor behavior (Barmack and Yakhnitsa, 2008). Interestingly, basket cells project in the sagittal plane (Palay and Chan-Palay, 1974), which is intriguing because Purkinje cell molecular and functional heterogeneity are restricted to sagittal domains (Apps et al., 2018). Here, we investigated basket cell connectivity based on how the pericellular baskets and pinceau terminals, in particular, are connected within Purkinje cell sagittal maps (Miterko et al., 2018b). This missing information is crucial for understanding how basket cells communicate with Purkinje cells, especially since the basket cells are coupled in sagittal rows (Sotelo, 2015). The electrical and chemical connectivity coefficients of basket cells are strongly represented in the sagittal plane (Rieubland et al., 2014). However, it is unclear how this functional organization fits into that of the broader cerebellar map with its complex but systematic patterns of topographic connectivity (Apps et al., 2018).

Cerebellar circuit maps are comprised of hundreds, perhaps thousands, of modules (Apps et al., 2018; Miterko et al., 2018b). Each module is assembled from an array of cell types that are arranged around Purkinje cell patterns (Sillitoe and Joyner, 2007; Apps and Hawkes, 2009). The surrounding cells are all patterned and include excitatory granule cells and unipolar brush cells (Sillitoe et al., 2003; Chung et al., 2009; Lee et al., 2015), inhibitory Golgi cells (Sillitoe et al., 2008), and even Bergmann glia (Reeber et al., 2018). Excitatory climbing fiber and mossy fiber afferents also terminate in domains that respect Purkinje cell zones (climbing fibers–Gravel et al., 1987; Sugihara and Shinoda, 2007; Reeber and Sillitoe, 2011; mossy fibers–Brochu et al., 1990; Quy et al., 2011; Gebre et al., 2012). In this study, we address whether molecular layer inhibitory interneurons are also patterned into zones. We use conditional genetic labeling and neuronal silencing in mice to uncover a size-based segregation of basket cell projections into

zones. We reveal that basket cell pinceaux have different sizes, and their sizes are determined cell non-autonomously by Purkinje cell activity. These data are critical for establishing a complete *in vivo* model for how the cerebellum functions during motor and cognitive tasks.

Results

Cerebellar basket cell interneurons have a complex structural interaction with Purkinje cells

The cerebellar nuclei mediate the motor and non-motor functions of the cerebellum using ascending and descending projections to the thalamus, red nucleus, and inferior olive (Figure 1A). However, before the information is communicated out of the cerebellum, it is processed in the cerebellar cortex by a relatively small number of excitatory and inhibitory neuron classes (Figure 1A). The cerebellar cortex has three distinct layers (Figure 1A). The most superficial layer contains inhibitory interneurons called basket cells and stellate cells, as well as excitatory climbing fibers and parallel fibers (the axons of granule cells). All four cell types project onto the Purkinje cells, which make up the middle cerebellar cortical layer called the Purkinje cell layer. The Purkinje cell layer also contains candelabrum cells and large astrocytes called Bergmann glia. The Purkinje cells perform the main computations in the cerebellum. The deepest layer is called the granular layer and it contains millions of excitatory neurons called granule cells, a smaller population of excitatory neurons called unipolar brush cells, inhibitory Lugaro cells and input fibers called mossy fibers that deliver sensory signals to the cerebellum from dozens of brain and spinal cord nuclei (Figure 1A; White and Sillitoe, 2013). The interactions between cerebellar cortical neurons depend on their individual cellular structures as well as their patterning in the coronal and sagittal planes. Here, we focus on the underappreciated architecture, patterning, and connectivity of the basket cells (Figure 1B).

Staining using a modified version of the Golgi-Cox method reveals the dense axonal projections of the basket cells around Purkinje cells (Figure 1B). The descending branches of basket cell axons enwrap the cell body of Purkinje cells, making perisomatic synapses, but they also extend

to reach the axon initial segment. A remarkable feature of this GABAergic innervation of Purkinje cells is the basket cell pinceau, a peculiar assembly of basket cell axons around the axon initial segment of Purkinje cells (Ramón y Cajal, 1911; Palay and Palay, 1970). With the prediction that the same organization is found in all regions of the cerebellum, we used HCN1 to examine basket cell connectivity in more detail. HCN1, Hyperpolarization Activated Cyclic Nucleotide Gated Potassium Channel 1, is a membrane protein that contributes to native pacemaker currents in the heart and nervous system (Chang et al., 2019). The four HCN channels are encoded by the *HCN1-4* genes and together they modulate cellular excitability, rhythmic activity, dendritic integration, and synaptic transmission (Moosmang et al., 1999; Moosmang et al., 2001; Notomi and Shigemoto, 2010; He et al., 2014). In the cerebellum, HCN1 is expressed in Purkinje cells where it mediates a large hyperpolarization-activated current (I_h) (Nolan et al., 2003). However, it is also heavily expressed presynaptically in basket cell terminals (Santoro et al., 1997; Lujan et al., 2005). Unexpectedly, we found that HCN1 shows a non-uniform pattern of expression on tissue sections cut through the adult mouse cerebellum (two different areas of cerebellar cortex are shown in Figure 1C). The unequal distribution of HCN1 around the base of Purkinje cells suggests that some basket cells either express more HCN1 or express it at higher intensity, compared to their neighbors. The patchy staining also raised the possibility that presynaptic HCN1 is expressed in a systematic pattern in the cerebellum. We therefore used a combination of marker analyses and genetic manipulations to test these different possibilities.

HCN1 expression in basket cell terminals respects the zonal patterning of Purkinje cells

The heterogeneous distribution of HCN1 at basket cell terminals hinted at a possible zonal pattern of expression in which some basket cells might express more HCN1 than others, or at the

153 extreme, some express it whereas others do not. Cerebellar zonal patterning is a fundamental
154 architecture that is respected not only by Purkinje cells, but also by their afferent and interneuron
155 microcircuit components (Apps and Hawkes, 2009; Cerminara et al., 2015). The precision of
156 zonal connectivity provides a structural framework for understanding how circuits operate during
157 ongoing motor function and motor learning (Attwell et al., 1999; Wadiche and Jahr, 2005; Horn
158 et al., 2010; Mostofi et al., 2010; Cerminara and Apps, 2011; Graham and Wylie, 2012).
159 Importantly, the behavioral correlates of zonal circuitry may be determined at the level of
160 cellular firing activity (Zhou et al., 2014; Xiao et al., 2014), and indeed if Purkinje cell activity is
161 manipulated, zonal patterning is disrupted (White et al., 2014). Based on these data, the growing
162 assumption is that all cerebellar components are zonally patterned, but we have only limited
163 experimental evidence for such organization for certain cell types. Of specific relevance, based
164 on Golgi-Cox staining we previously demonstrated the possibility that stellate cell interneurons,
165 specifically their somata, are restricted at Purkinje cell zonal boundaries in the molecular layer
166 (Sillitoe et al., 2008). However, based on the randomness of staining using the Golgi-Cox
167 method and the limited ability to track distinct subsets of cells and their respective projections
168 with full clarity, we could not with confidence make any conclusion about how basket cells are
169 organized (Sillitoe et al., 2008). The potential of HCN1 expression to fill this gap in our
170 knowledge motivated a double-staining experiment using HCN1 and zebrinII (Figure 2).
171 ZebrinII is a polypeptide antigen found on the aldolaseC protein (Ahn et al., 1994; Brochu et al.,
172 1990). Lobules I-V and anterior VIII-IX are identified by a striking array of zebrinII zones,
173 where lobules VI-VII and posterior IX-X express it uniformly (Sillitoe and Hawkes, 2002). We
174 therefore analyzed HCN1 expression in lobule VIII due to the clarity of the individual zones
175 (Figure 2A) as defined by the sharpness of zonal boundaries (Figure 2B) and because the zones

abutting the P1+ midline zone in lobule VIII are roughly equal in width; the number of Purkinje cells in a zebrinII expressing zone is equal to the number of Purkinje cells in an adjacent zone that does not express the antigen (Brochu et al., 1990; Ozol et al., 1999). We found that the pattern of HCN1 indeed respected the pattern of zebrinII, with an inverse relationship between the two. HCN1 expression was more prominent around Purkinje cells that did not express zebrinII (Figure 2C-F), with this relationship best appreciated at zone boundaries where zebrinII non-expressing cells have a robust HCN1 profile compared to the immediately adjacent zebrinII expressing cells that have reduced prominence of HCN1 profiles (Figure 2D, F). We next tested whether the HCN1 expressing profiles were different sizes. Specifically, we tested whether there is restricted expression of the protein, or differences in the intensity of expression but within equal sized profiles around Purkinje cells. We quantified pinceau expression in the P1+ to P3+ zones (and intervening P- zones) of lobule VIII (Figure 2H) and found a significant difference in the size of pinceaux between zebrinII-positive and zebrinII-negative zones (Figure 2I). We then tested whether this size difference was driven by an unequal intensity of protein expression. We found no difference in HCN1 intensity between pinceaux of different sizes (Figure 2J). Although we focused our analysis on the vermis, we also observed a similar patterning of HCN1 into parasagittal zones in the hemisphere lobules (Figure 2 – Figure Supplement 2). These data suggested that zebrinII-positive zones were populated with basket cells with small pinceaux, while zebrinII-negative zones were populated with basket cells with large pinceaux (Figure 2G).

However, zebrinII is not the only marker of zones (White and Sillitoe, 2013). In some cases, zebrinII zones are complementary to the expression pattern of proteins such as phospholipase C β4 (PLCβ4; Armstrong and Hawkes, 2000; Sarna et al., 2006), while in other cases they are co-

expressed with proteins such as phospholipase C β3 (PLCβ3; Armstrong and Hawkes, 2000; Sarna et al., 2006). We therefore co-stained coronal cut tissue sections with HCN1 and PLCβ4 (Figure 3A-F) and found that indeed, larger HCN1 expressing basket cell profiles localized around PLCβ4 expressing/zebrinII non-expressing Purkinje cells (P- zones in Figure 3G-H).

In addition to complementary patterns of expression in lobules with zebrinII zones, there are also markers that label zones within lobules with Purkinje cells that all express zebrinII. Lobules VI-VII and posterior IX-X express the small heat shock protein HSP25 in zones (Armstrong et al., 2000), and we showed that the pattern of Neurofilament Heavy Chain (NFH) expression is complementary to HSP25 in these specific lobules (Demilly et al., 2011). In addition, because NFH reveals zones across multiple sets of lobules (Demilly et al., 2011; White and Sillitoe, 2013) and because the robustness of NFH within both the Purkinje cells and the "basket", or somata portion of the basket cell itself (Figure 4J) allows particularly evident distinction of zones in the region relevant to basket cells, we used it to test whether HCN1 basket cell zones extend beyond the limits of lobule VIII (Figure 4). After co-staining with HCN1 and NFH, we found that zones with high NFH expression correspond to distinct HCN1 zones in lobule VII (Figure 4A-C) and maintain that relationship through lobules VIII (Figure 4D-F) and IX (Figure 4G-I).

Different commonly used basket cell markers are in fact expressed in zones

In addition to HCN1, cerebellar basket cell pinceaux express a variety of molecular markers, and among these are Kv1.1 (Wang et al., 1994; Iwakura et al., 2012), PSD95 (Fukaya and Watanabe, 2000; Sivilia et al., 2016), and GAD67 (Iwakura et al., 2012; Sivilia et al., 2016). We first set out to confirm that each protein shared a similar sub-cellular compartment within the basket cells

specifically in lobule VIII by co-staining with HCN1. We found that in all cases, the pinceaux were robustly co-stained and shared an identical expression localization (Kv1.1 Figure 5A-F; PSD95 Figure 5G-L; GAD67 Figure 5M-R). We next tested whether these three additional markers are also heterogeneously distributed around Purkinje cells. Similar to HCN1, we found that Kv1.1, PSD95, and GAD67 all adhere to the zonal boundaries, as assessed on coronal cut tissue sections from lobule VIII (Figure 6A-B). Purkinje cells with large versus small pinceaux, as defined by marker expression in the pinceau, established clear-cut boundaries (dotted lines in Figures 5 and 6). Interestingly, all four markers revealed an identical staining pattern; that is, all four basket cell markers delineated the same spatial expression pattern, in the same zones.

The zonal patterning of basket cell projections is based on the size of their pinceaux

Despite their diverse functions, all four proteins have the same zonal pattern. This is peculiar given that the Purkinje cell map, which consists of complex arrays of interdigitating patterns, is thought to instruct the formation of its afferent microcircuits (Miterko et al., 2018). Therefore, unlike zebrinII, and the two dozen plus known markers that form a molecular map, we tested the alternate possibility that perhaps basket cells zones represent a more fundamental feature of the circuit, its anatomy. To test this hypothesis, we used a genetic fate mapping approach to selectively mark basket cells and specifically to highlight the boundaries of their cell membranes with a conditional reporter (Figure 7). We recently showed that an *Ascl1*^{CreERT2} allele can be used to mark basket cells based on their birth date during late embryogenesis (Brown et al., 2019). *Ascl1*, also known as *Mash1*, encodes a member of the basic helix-loop-helix (BHLH) family of transcription factors. A knock-in allele of *CreER* into the *Ascl1* locus faithfully reports on the differentiation of GABAergic neurons in the cerebellum, and it has a dual function in labeling

different subsets of inhibitory neurons at the time of their birth (Sudarov et al., 2011). Here, we crossed the *Ascl1*^{CreERT2} mice to a mouse line that expresses myristoylated GFP (mGFP) in differentiated neurons (Hippenmeyer et al., 2005), but only after recombination is induced upon tamoxifen administration to the mice (Brown et al., 2019). We chose this genetic strategy because oral gavage of tamoxifen to pregnant dams when their embryos are embryonic day (E) 18.5 labels a rich population basket cells with recombination at ~43% across the entire cerebellum (Brown et al., 2019; the genetic strategy is schematized in Figure 7E), and the mGFP reporter impressively fills the entire axons of even the finest projections in the cerebellum (Sillitoe et al., 2009). After inducing basket cell recombination during development, we followed the marked cells into adulthood to examine their architecture using triple staining with a pan Purkinje cell marker, GFP expression, and a Purkinje cell zone marker. The IP3R1 receptor uniformly marks Purkinje cells (Figure 7A), whereas the genetically marked basket cell pinceaux delineate a sharp boundary within the Purkinje cell layer (Figure 7B). The dotted line in Figure 7B separates the pinceaux into 1) a large subset with prominent profiles around the base of the Purkinje cells and extending deeper into the granular layer onto the initial segment of the Purkinje cell axons (larger open bracket, left in Figure 7B) and 2) a small subset with less prominent profiles, but that nevertheless adopts the same architectural connectivity with the Purkinje cells (smaller open bracket, right in Figure 7B). Labeling with PLCβ4 demonstrates that the division of basket cell projections respects the boundaries of the Purkinje cell zones (Figure 7C). However, compared to the strict and uncompromising relationship between climbing fibers and Purkinje cells (Gravel et al., 1987; Voogd and Ruigrok, 2004; Pijpers et al., 2006; Sugihara et al., 2007; Reeber and Sillitoe, 2011; Reeber et al., 2013), the basket cell to Purkinje cell topography is not perfect at the zonal boundary (Figure 7D). It is perhaps more reminiscent of

the mossy fiber to Purkinje cell topography that shows an obvious pattern of zones, although the relationship at the boundaries is more complex (Brochu et al., 1990; Pakan et al., 2010; Sillitoe et al., 2010; Ruigrok, 2011; Reeber et al., 2011). Mossy fiber zones often extend beyond the boundaries defined by the Purkinje cell zones. Still, quantification of the basket cell pinceaux using GFP fluorescence genetic marking confirms that as a population, the patterning of the pinceaux into zones reflects a significant difference in their sizes between zones (Figure 7F). Interestingly, the genetic marking strategy labeled collateral fibers in the granular layer that are also restricted to Purkinje cell zones (see granular layer in Figure 7B). The collaterals are prominent below the PLCβ4-expressing zones with little to no labeling in PLCβ4 negative zones.

Purkinje cell neurotransmission controls the segregation of basket cell projections into zones with large and small pinceaux

The establishment of Purkinje cell zones is dependent on a sequential (but overlapping) series mechanisms involving their birth date (Hashimoto and Mikoshiba, 2003, Namba et al., 2011), molecular identity (Croci et al., 2006), patterning (Baader et al., 1999; Sillitoe et al., 2008), and cell migration (Larouche et al., 2008). The patterning of afferents is also dependent on these Purkinje cell molecular processes (Sillitoe et al., 2010). At the level of specific cell-to-cell connections, distinct molecular mechanisms also control basket cell targeting. The targeting of basket axons to the axon initial segment depends on Semaphorin3A (Sema3A) and its receptor neuropilin-1 (NRP1; Telley et al., 2016). Sema3A is secreted by Purkinje cells, which attracts the basket cell axons that express NRP1 toward the initial segment. NRP1 also mediates subcellular cell-to-cell recognition through a trans-synaptic interaction with neurofascin 186 (NF 186), a cell adhesion molecule of the L1 immunoglobulin family that is required for the formation and

maintenance of the pinceau (Ango et al., 2004, Zonta et al., 2011, Buttermore et al., 2012). However, even though basket cells are born during embryogenesis (see Figure 7E), functional basket cell connections are formed postnatally (Sotelo, 2008), a period when neuronal activity starts to remodel the cerebellar wiring diagram for function (Kano and Watanabe, 2019). Indeed, the molecular genetics and morphogenetic programs act cooperatively with neuronal activity to shape afferent patterning (Tolbert et al., 1994), and Purkinje cells specifically guide them into precise zones (White et al., 2014). We therefore tested whether Purkinje cells also instruct the zonal patterning of basket cell pinceaux. GABAergic neurotransmission is selectively silenced in Purkinje cells of *Pcp2*^{Cre};*Slc32a1*$^{flox/flox}$ mice (White et al., 2014). This particular *Pcp2*^{Cre} allele is ideal for our purpose because it expresses *Cre* during embryogenesis and continues into adulthood (Lewis et al., 2004), which means that even the developing Purkinje cells lack *Slc32a1* after recombination occurs with the *floxed* allele (Tong et al., 2008). In these mutants, Purkinje cells are capable of receiving signals and firing simple spikes and complex spikes, although they cannot communicate their computations downstream (White et al., 2014; Stay et al., 2019). Compared to control *Slc32a1*$^{flox/flox}$ mice (*Cre*-negative, no *Slc32a1* deletion; Figure 8A,C,E), the mutants that lack *Slc32a1* in Purkinje cells do not have a clear distinction of Purkinje cell zones or HCN1 zones, as defined by the basket cell pinceaux (Figure 8B, D, F). Instead, we observed a uniform distribution of HCN1, suggesting that basket cell pinceaux are all approximately the same size in the mutants. Quantification of pinceau size based on HCN1 expression confirmed that Purkinje cell neurotransmission is required for basket cell size diversity, and is the basis of their zonal plan (Figure 8G). Without Purkinje cell activity, all basket cell pinceaux were not significantly different in size compared to control pinceaux within zebrinII-positive zones

(Figure 8G). These data suggest that Purkinje cell activity influences basket cell diversity by sculpting pinceau structure and designating them into large versus small subsets.

We next asked whether the activity at basket cell to Purkinje cell synapses might also play a role in instructing the Purkinje cell zonal patterns. Specifically, we asked: if the Purkinje cell map controls both the genetic programs as well as the activity required for zonal patterning, then can the afferents also contribute to the shaping of the Purkinje cell map that they integrate into? To address this question, we again used the *Ascl1*^{CreER} allele (Sudarov et al., 2011), but this time we crossed it to the *Slc32a1*$^{flox/flox}$ line (Tong et al., 2008) in order to block inhibitory neurotransmission from basket cells to Purkinje cells by delivering tamoxifen to E18.5 pups *in utero* (Brown et al., 2019). We then stained Purkinje cells for zebrinII and revealed that the zonal plan (Figure 9A) was indistinguishable when compared to the patterns of zones in different lobules from the anterior, central, posterior, and nodular domains (Figure 9B) between controls (Figure 9C; *CreER* is not expressed because the mice do not have the allele, and as a result *Slc32a1* is left intact, although like the mutants, the control mice are also given tamoxifen) and mutants (Figure 9D). Therefore, inhibitory basket cell output does not control the anterior-posterior or medial-lateral patterning of molecular markers in the Purkinje cells. These data also confirm that Purkinje cell activity restricts basket cells into a highly patterned zonal map, with a key anatomical substrate of connectivity established by segregating pinceaux into distinct sizes.

Discussion

The cerebellum is organized into a fundamental map of zones defined by molecular expression patterns, neuronal firing properties, behavioral outputs, and even disease phenotypes. Purkinje cells are at the center of each zone, receiving precisely mapped inputs from excitatory climbing fibers and mossy fibers. Here, we demonstrate that the inhibitory projections from basket cells onto Purkinje cells are also patterned into zones. We identify that HCN1, Kv1.1, PSD95, and GAD67 are all expressed in basket cell pinceaux and uncover a pattern of zones in the adult cerebellum. However, their expression reveals a unique feature of cerebellar topography: their zonal patterning is defined by the sizes of the basket cell pinceaux, rather than spatial differences in protein expression. We tested whether Purkinje cells drive the topography of inhibitory projections, as they do for excitatory afferents. Interestingly, altering Purkinje cell activity eliminated the division of basket cells into large and small zones. Our data demonstrate that basket cell projections are topographically organized, and that their patterning is dependent on proper activity in the cerebellar cortex. The results provide a neural substrate for how cerebellar circuitry might control module-specific firing properties and encode diverse behavioral outputs.

The finer details of cerebellar patterning have been unveiled using protein expression (Hawkes and Leclerc, 1987), mRNA expression (Millen et al., 1995), viral marking (Hashimoto and Mikoshiba, 2003), transgenic alleles (Furutama et al., 2010; Fujita et al., 2010), and conditional genetic labeling (Sillitoe et al., 2009) and, in addition, the topography of afferents has been studied using injection approaches of neural tracing (Sugihara and Quy, 2007), genetically encoded neural tracers (Braz et al., 2002), and genetically encoded reporters (Hantman and Jessell, 2010). However, the initial motivations to study cerebellar patterns were based purely on

anatomical analyses; Jan Voogd expanded on the initial finding of Verhaart (1956) who used the Häggqvist myelin stain to reveal small, medium, and large caliber axons in the brachium conjunctivum. Voogd demonstrated the presence of white matter compartments that contained large myelinated axons which were separated by narrow bands of small fibers. Some key features he studied further were the continuity of compartments across subsets of lobules, and that the compartments housed the axons of Purkinje cells that were topographically linked to specific cerebellar nuclei (Voogd, 1964). Within the cerebellar cortex, Hawkes and colleagues also revealed a compartmental division of the cerebellum that was based on anatomy, showing that after a particular preparation of the tissue, the granular layer forms “blebs” that respect the boundaries of zebrinII expression (Hawkes et al., 1997). Our data integrates the molecular properties of basket cell pinceaux with their connectivity to Purkinje cell axons, unmasking a fundamental level of zonal patterning that segments basket cell projections based on their sizes. Interestingly, although the authors did not discuss it, PLCβ1 expression shows predominant basket cell staining particularly around PLCβ4-expressing Purkinje cells (Fukaya et al., 2008). We predict that markers that have a seemingly uniform expression in basket cells should in fact reveal cerebellar zones based on pinceau size, although we do not exclude the possibility that some molecules may be expressed in patterns of basket cells, irrespective of their zonal sizes.

The zonal topography of the pinceaux raise a critical functional question: how does basket cell heterogeneity impact cerebellar function? Multiple lines of experimental evidence using different model systems suggest a role for zones during behavior (Schonewille et al., 2006; Horn et al., 2010; Cerminara and Apps, 2011; Graham and Wylie, 2012; Long et al., 2018), and these studies were supported by electrophysiological analyses indicating that synaptic plasticity may be

379 determined by zone-specific properties (Wadiche and Jahr, 2005; Paukert et al., 2010). More
380 recently, it has been uncovered that systematic differences in the function of zones could be
381 hard-wired into the basic firing properties of Purkinje cells. ZebrinII-positive Purkinje cells were
382 reported to have lower frequencies and more regularity, whereas zebrinII-negative Purkinje cells
383 have a higher firing frequency and a more irregular pattern of activity (Zhou et al., 2014; Xiao et
384 al., 2014). Moreover, consistent with the highly organized convergence of mossy fibers and
385 climbing fibers within dedicated zones (Voogd et al., 2003), *in vivo* electrophysiology recordings
386 demonstrate zone-specific interactions in simple spike and complex spike activity (Tang et al.,
387 2017). Interestingly, during development there is a converse relationship such that Purkinje cell
388 activity itself is required for precisely shaping the zones into fine-grained compartments (White
389 et al., 2014). With the various classes of interneurons following the zonal scheme (Consalez and
390 Hawkes, 2013), and the data presented in this study, it could be that Purkinje cells use
391 developmental mechanisms to establish their own behaviorally relevant specializations, and for
392 basket cells, this means their segregation into size-specific zones. It is suggested that Purkinje
393 cells zones may have discrete requirements during LTD (long-term depression) versus LTP
394 (long-term potentiation) (Wu et al., 2019). ZebrinII-positive zones are predicted to have a major
395 role in behaviors such as the vestibulo-ocular reflex, which is heavily dependent upon LTP,
396 whereas as behaviors such as eye-blink conditioning may be more dependent on LTD. We know
397 that at least some portion of the eye blink conditioning circuit is restricted to zebrinII-negative
398 zones (Attwell et al., 1999; Attwell et al., 2001; Mostofi et al., 2010). By extrapolation, the large
399 pinceaux in the zebrinII-negative zones then could serve to more strongly modulate the high
400 frequency firing and more irregular activity of Purkinje cells during learning. Interestingly,
401 optogenetic stimulation of basket cells in the deep paravermis of mouse lobule V/VI, a

predominantly zebrinII-negative domain, strongly modulated the timing of the blink (Heiney et al, 2014). In addition, though, selective elimination of basket cell output results in an increase in Purkinje cell simple spike frequency (Brown et al., 2019). Together, these data indicate that basket cells may not set the normal firing rate of Purkinje cells, but instead might provide a custom brake. Therefore, Purkinje cells may determine the strength of their own innervation, which could ensure that the circuit is equipped to accommodate certain behaviors. Loss of *Slc32a1* in Purkinje cells obscures the zonal pattern, and therefore alters learning on rotarod (White et al., 2014). We propose that the establishment of neural activity and the formation of topographic patterns is tightly linked to the control of behavior in mature animals. However, we note that HCN1, Kv1.1, and PSD95 are all activity dependent (Arimitsu et al., 2009; Grosse et al., 2000; Lu et al., 2004; Subramanian et al., 2019). What, then, does the silencing of Purkinje cell output activity tell us about how basket cells acquire a nonuniform pattern/size (Figure 8G)? Silencing Purkinje cell GABAergic output likely abolishes the patterned distribution of basket cell projections as a consequence of masking Purkinje cell identities, resulting in no pinceau specificity and an accompanying adjustment in protein expression patterns (Figure 8A-F).

There are several possibilities for how the adjustments in basket cell projection size might take effect when Purkinje cell neurotransmission is blocked. It could be that silencing Purkinje cells changes the convergence of basket cell axons. In control mice, 3-7 basket cells typically converge onto each Purkinje cell (Palay and Chan-Palay, 1974). Silencing Purkinje cell output, a physiological cue that segregates the projections into zones (Figure 8), could result in fewer average basket cell projections per Purkinje cell. Alternatively, the loss of Purkinje cell signals may eliminate a growth signal that either increases the extent of innervation from some fibers

and/or restricts the size of others into large versus small projection domains. Moreover, it could be that the loss of Purkinje cell output does not change the average size or number of primary ascending and descending basket cell fibers; instead, the collateralization of smaller endings at the Purkinje cell initial segment may be defective (Sotelo, 2008), and perhaps more so in what would develop into the larger pinceaux. The mutant mice may have a lack of axonal refinement. Purkinje cell activity therefore instructs the local precision of extracerebellar and intracerebellar afferent projections (White et al., 2014). *In vivo*, it is likely that multiple steps are required for proper basket cell targeting onto Purkinje cells. The directional growth of basket cell projections from the soma to the axon initial segment requires an ankyrinG-dependent subcellular gradient of neurofascin186 (NF186) (Ango et al., 2004). NF186 is expressed on Purkinje cells and trans-synaptically interacts with neuropilin-1 (NRP1), a Semaphorin receptor expressed by basket cells, to control the formation of pinceau synapses (Telley et al., 2016). Here, we show that there is an added level of specificity, in a process that restricts pinceau formation according to size. We argue that Purkinje cell activity controls the distinction of basket cells by size, and although basket cell GABAergic activity contributes to postnatal climbing fiber synapse elimination (Nakayama et al., 2012), it does not play a role in patterning Purkinje cell zones (Figure 9).

The electrical and chemical connectivity of the molecular layer interneurons are highly structured, with connectivity clustering coefficients that reflect a spatial arrangement in sagittal rows (Rieubland et al., 2014). Electrical connections tether rodent basket cells into groups of 5 (Alcami and Marty, 2013). It could be that the local electrical networking, their arrangement into rows, and their size selectivity fall into a singular map, following the “one-map hypothesis” proposed by Apps and Hawkes (Apps and Hawkes, 2009). It is interesting to speculate how such

448 a model could benefit from basket cell patterns. Cortical output is modulated by climbing fiber
449 and parallel fiber input as well as the intrinsic firing of Purkinje cells. However, since basket
450 cells contribute to the excitation/inhibition (E/I) balance, and since glutamate spillover from
451 climbing fibers impacts molecular layer interneuron function (Szapiro and Barbour, 2007), it is
452 possible that the different sizes of basket cell projections (namely their pinceux, although likely
453 their full innervation) uniquely complement the excitatory innervation. Together, they could
454 drive cerebellar module function (Wu et al., 2019) and synchronous activity (Welsh et al., 1995),
455 but also direct the precision of synaptic plasticity (Wadiche and Jahr, 2005; Paukert et al., 2010).
456

Conclusions

Cerebellar basket cells are a class of molecular layer interneurons that project to Purkinje cells. We found using several different molecular markers that basket cell pinceaux are organized into zones that coincide with the pattern of a well-established Purkinje cell map. We used an *Ascl1*^{CreERT2} genetic inducible allele to leverage the spatial and temporal pattern of inhibitory interneuron development in order to mark the terminal field topography of basket cells. We reveal that basket cells are patterned according to the size of their pinceaux, which innervate the Purkinje cell axon initial segment. Additionally, we found that Purkinje cell GABAergic activity is required for the cell non-autonomous patterning of basket cell pinceaux. This study uncovers a fundamental zonal architecture of cerebellar interneuron projections and illustrates that basic neuroanatomical connectivity provides the underlying guiding principle for organizing the brain.

Ethics

Animal experimentation: All animals were housed in an AALAS-certified facility on a 14hr light cycle. Husbandry, housing, euthanasia, and experimental guidelines were reviewed and approved by the Institutional Animal Care and Use Committee (IACUC) of Baylor College of Medicine (protocol number: AN-5996).

Materials and Methods

Animal maintenance. Mouse husbandry and experiments were performed under an approved Institutional Animal Care and Use Committee (IACUC) protocol at Baylor College of Medicine (BCM). Male and female mouse genetic models (see below the details for the different alleles) were obtained from The Jackson Laboratory (Bar Harbor, ME, USA) and a colony was established and thereafter maintained in house at BCM. We bred mice using standard timed pregnancies, and noon on the day a vaginal plug was detected was considered embryonic day (E) 0.5. The day of birth was designated as postnatal day (P) 0. Mice of both sexes were studied. All mice used in this study were mature adults, with their ages ranging between 3 to 14 months old.

Genetically engineered mouse lines. Three mouse lines were intercrossed to generate the alleles used in this study. The first line exhibits silenced Purkinje cell neurotransmission by elimination of the vesicular GABA transporter (*Slc32a1*, also known as *Vgat)* under the control of the Purkinje cell-specific *Pcp2* (also known as *L7*) promoter. $Pcp2^{Cre};Slc32a1^{flox/flox}$ mice were generated as previously described (White et al., 2014). $Pcp2^{Cre}$ mice (Lewis et al., 2004) were crossed with a conditional "floxed" allele of *Slc32a1* (Tong et al., 2008). *Slc32a1* is widely expressed in GABAergic and glycinergic neurons in the brain and it is essential for loading GABA into presynaptic vesicles for fast inhibitory neurotransmission (McIntire et al., 1997; Chaudhry et al., 1998; Fujii et al., 2007; Saito et al., 2010). Genotyping for the $Pcp2^{Cre}$ allele was performed using standard *Cre* primers (Sillitoe et al., 2008, 2010), and genotyping for the $Slc32a1^{flox}$ allele was performed according to Tong et al. (2008). The control mice used for the genetic manipulations were littermate controls from the $Slc32a1^{flox}$ strain, lacking *Cre* and therefore with preserved *Slc32a1* functioning, and are referred to as

498 *Slc32a1*$^{flox/flox}$ in this study. The second mouse line has a genetically encoded fluorescent tag that
499 we used to determine the size of projections. The mice have myristoylated green fluorescent
500 protein (mGFP) knocked-in to the Tau locus (Hippenmeyer et al., 2005) with an upstream floxed
501 transcriptional stop cassette as well as a knock-in allele of the *CreER*^{T2} cassette under the control
502 of the *Ascl1* (or *Mash1*) promoter (*Ascl1*^{CreERT2};*Tau*$^{flox\text{-}stop\text{-}mGFP\text{-}lacZ}$). To genetically label basket
503 cells specifically, tamoxifen was administered to pregnant dams at E18.5, a time point at which
504 subsets of basket cells emerge during embryogenesis (Sudarov et al., 2011). Genotyping
505 procedures for the *Ascl1*^{CreERT2} and the *Tau*^{mGFP} alleles were performed according to the
506 protocols described in Sillitoe et al. (2009). The third line of mice exhibits silenced basket cell
507 inhibitory neurotransmission by elimination of *Slc32a1* under the control of the *Ascl1* promoter
508 driving *CreER*^{T2} expression (*Ascl1*^{CreERT2};*Slc32a1*$^{flox/flox}$). To selectively target the deletion of
509 *Slc32a1* in only basket cells, tamoxifen was administered to pregnant dams at E18.5. Genotyping
510 for the *Slc32a1*^{flox} conditional allele was performed according to a standard polymerase chain
511 reaction protocol as described in Brown et al. (2019) and originally developed by Tong et al.
512 (2008). Additional C57BL/6J controls were used for the initial analyses of patterns.
513
514 *Cre induction.* Tamoxifen (Sigma-Aldrich catalog #T5648) was dissolved on a rocker at 37°C
515 overnight in fresh corn oil (not older than 5 months old, stored in the dark at room temperature)
516 at a concentration of 20 mg/ml (Sillitoe et al., 2009; Zervas et al., 2004). An 18-gauge needle
517 was fitted onto a Luer-Lok syringe, which was used to gently pipette the solution up and down 3-
518 5 times in order to dissolve any remaining clumps of tamoxifen. To improve pup survival when
519 targeting the basket cells, we administered a mixture of 200 μg/g tamoxifen supplemented with
520 50 μg/g progesterone to the pregnant dams by oral gavage at E18.5 (Sudarov et al., 2011; Bowers

et al., 2012). The full procedure for targeting the basket cells with tamoxifen was described in Brown et al. (2019). We tested the reliability of detecting the genetically marked cells by examining the cerebella of *CreER*^{T2}-negative mice (Figure 7 – Figure Supplement 1).

Immunohistochemistry. Perfusion and tissue fixation were performed as previously described (Sillitoe et al., 2008a). Briefly, mice were anesthetized by intraperitoneal injection with Avertin (2, 2, 2-Tribromoethanol, Sigma-Aldrich catalog # T4). Cardiac perfusion was performed with 0.1 M phosphate-buffered saline (PBS; pH 7.4), then by 4% paraformaldehyde (4% PFA) diluted in PBS. For cryoembedding, brains were post-fixed at 4°C for 24 to 48 hours in 4% PFA and then cryoprotected stepwise in sucrose solutions (15% and 30% diluted in PBS) and embedded in Tissue-Tek O.C.T. compound (Sakura Finetek USA; catalog #4583). Tissue sections were cut on a cryostat with a thickness of 40 µm and individual free-floating sections were collected sequentially and immediately placed into PBS. Our procedures for immunohistochemistry on free-floating frozen cut tissue sections have been described extensively in previous work (Sillitoe et al., 2003, 2010; White and Sillitoe, 2013a; White et al., 2014; White and Sillitoe, 2017). However, below we describe the reagents used in this study. After completing the staining steps, the tissue sections were placed on electrostatically coated glass slides and allowed to dry.

Purkinje cell zone and basket cell projection markers. Monoclonal anti-zebrinII (Brochu et al., 1990) was used directly from spent hybridoma culture medium at a concentration of 1:250 (gift from Dr. Richard Hawkes, University of Calgary). ZebrinII recognizes an antigen on the aldolaseC protein (Ahn et al., 1994) and it is a well-established marker for Purkinje cell zones. Rabbit polyclonal anti-phospholipase C β4 (PLCβ4; 1:150; Santa Cruz Biotechnology; catalog #sc-20760) was used to label Purkinje cell zones that are complementary to those revealed by

ZebrinII (Sarna et al., 2006). Neurofilament heavy chain (NFH) is also expressed in Purkinje cell zones, although it shows an additional level of zonal complexity (Demilly et al., 2011; White and Sillitoe, 2013). Mouse monoclonal anti-NFH (1:1,000; MilliporeSigma; catalog #NE1023) was used to label the soma, dendrites, and axons of adult Purkinje cells, as well as the axons and terminals of basket cells. We also used goat polyclonal anti-inositol 1,4,5-trisphosphate receptor type 1 (IP3R1; 1:250; Santa Cruz Biotechnology; catalog #sc-6093) and rabbit polyclonal anti-calbindin (1:1,000; Swant; catalog #300) as general markers to label all adult Purkinje cells. Rabbit polyclonal anti-hyperpolarization-activated cyclic nucleotide-gated channel 1 (HCN1; 1:350; Synaptic Systems), was used to label basket cell axons and pinceau terminals. Postsynaptic density protein 95 (PSD95) has been shown to have high expression in the presynaptic plexus of cerebellar basket cells (Kistner et al., 1993) and therefore mouse monoclonal anti-PSD 95 (1:500; UC Davis/NIH NeuroMab Facility; catalog #75-028) was used as another marker of basket cell projections. Potassium voltage-gated channel subfamily A member 1 (Kv1.1) is abundantly expressed in cerebellar basket cell axon terminals (Laube et al., 1996). Rabbit polyclonal anti-Kv1.1 (1:500; Alomone Labs; catalog #APC-009) was also used as marker of basket cell axons and terminals. Some tissue sections were double, triple, or quadruple-labeled with the different markers listed above, and in some cases with chicken anti-GFP (1:1,000; Abcam, catalog #AB13970) in order to visualize the mGFP reporter expression.

We visualized immunoreactive complexes either using diaminobenzidine (DAB; 0.5 mg/ml; Sigma) or fluorescent secondary antibodies. For the DAB reaction, we used horseradish peroxidase (HRP)-conjugated goat anti-rabbit and goat anti-mouse secondary antibodies (diluted 1:200 in PBS; DAKO) to bind the primary antibodies. Antibody binding was revealed by

incubating the tissue in the peroxidase substrate 3,3'-diaminobenzidine tetrahydrochloride (DAB; Sigma-Aldrich, catalog #D5905), which was made by dissolving a 100mg DAB tablet in 40ml PBS and 10 µL 30% H_2O_2. The DAB reaction was stopped with PBS when the optimal color intensity was reached. Staining for fluorescent immunohistochemistry was performed using donkey anti-mouse, anti-rabbit, or anti-guinea pig secondary antibodies conjugated to Alexa-350, -488, -555, and -647 fluorophores (1:1,500 for all; Invitrogen). Tissues sections were coverslipped using either Entellan mounting media (for DAB; Electron Microscopy Sciences) or FLUORO-GEL with Tris buffer (Electron Microscopy Sciences). We tested the specificity of the secondary antibodies by processing the tissue in the absence of primary antibodies. No signal was detected indicating that the staining we observed in basket or other cells was not due to nonspecific signals from the Alexa or HRP-conjugated antibodies. There was also no staining when the secondary antibodies were left out of the staining mixture (Figure 2 – Figure Supplement 2). Sample size was not determined using a priori power analysis, but was based on the criteria for significance in observations. A total of 50 cerebella from the 3 genotypes of mice were used in this study, which were processed for immunohistochemistry to examine pinceau patterning (detailed numbers of animals used for specific genotypes and cellular marker combinations are listed in the figure legends). From these 50 cerebella, images from 12 controls (*Slc32a1*$^{flox/flox}$), 4 with genetically labeled basket cells (*Ascl1*^{CreERT2};*Tau*$^{flox\text{-}stop\text{-}mGFP\text{-}lacZ}$), and 4 with silenced Purkinje cell neurotransmission (*Pcp2*^{Cre};*Slc32a1*$^{flox/flox}$) were analyzed for pinceau size and fluorescence differences using the quantification methods described below. An additional 4 cerebella were used for immunostaining controls (shown in the figure supplements).

589 *Golgi-Cox staining.* The brains from six control mice were removed from the skull and then
590 processed using the FD Rapid Golgi Stain Kit (PK 401 from FD Neurotechnologies, INC). We
591 focused the anatomy on optimally stained brains. All steps were carried out according to the
592 manufacturers' instructions. After staining, the tissue was dehydrated in an ethanol series,
593 cleared with xylene, and then mounted onto electrostatically coated glass slides with cytoseal.
594
595 *Imaging of immunostained tissue sections.* Photomicrographs of stained tissue sections were
596 captured with a Zeiss AxioCam MRm (fluorescence) and AxioCam MRc5 (DAB-reacted tissue
597 sections) cameras mounted on a Zeiss Axio Imager.M2 microscope or on a Zeiss AXIO
598 Zoom.V16 microscope. Apotome imaging (Apotome.2, Zeiss) of tissue sections was performed
599 and images acquired and analyzed using either Zeiss AxioVision software (release 4.8) or Zeiss
600 ZEN software (2012 edition). After imaging, the raw data was imported into Adobe Photoshop
601 CC 2019 and corrected for brightness and contrast levels. The schematics were drawn in Adobe
602 Illustrator CC 2019 and then imported into Photoshop to construct the full image panels.
603
604 *Quantification of the sizes of basket cell projections in Purkinje cell zones.* Basket cell pinceau
605 sizes within Purkinje cell zones were quantified using the Fiji distribution of ImageJ software
606 (Schindelin et al., 2012). Images of mGFP-tagged basket cell projections (mainly the "basket"
607 portion of the projection that sits at the base of the Purkinje cell soma and the obvious pinceau
608 terminal projection that resides on the Purkinje cell axon initial segment) overlaid with Purkinje
609 cell zonal markers (ZebrinII, PLCβ4, or NFH) were loaded into Fiji, and Purkinje cell zonal
610 boundaries within the image were identified. The Purkinje cell zonal marker channel was then
611 removed from the image so that only the mGFP-tagged basket cell projections remained. Each

image was subsequently set to a threshold of 19-20%, or until all baskets were clearly filled in the image. A 100 μm region of interest (ROI) containing only the mGFP-tagged baskets was selected from the previously marked Purkinje cell zone border, and the total area of the ROI covered by pinceaux was calculated using the "analyze particles" function. The resulting total basket-containing area within each analyzed zone was recorded in MS Excel. Two-sample t-tests comparing total basket areas between positive and negative Purkinje cell marker zones as well as graphical representations of the statistical results were generated using GraphPad Prism software version 7 (GraphPad Software, Inc). Descriptive statistics are listed in the figure legends for the relevant figures. For the control (C57BL/6J and *Slc32a1*$^{flox/flox}$) mice, 24 coronal cerebellar sections containing a total of 52 zebrinII-positive zones and 51 zebrinII-negative zones collected from 12 different mice were analyzed. In mice with genetically labeled basket cells (*Ascl1*^{CreERT2};*Tau*$^{flox\text{-}stop\text{-}mGFP\text{-}lacZ}$), 8 coronal cerebellar sections containing a total of 20 PLCß4-positive and 22 PLCß4-negative zones from 4 different mice were analyzed. For the mice with silenced Purkinje cell neurotransmission (*Pcp2*^{Cre};*Slc32a1*$^{flox/flox}$), 8 coronal cerebellar sections containing a total of 20 zebrinII-positive zones and 20 zebrinII-negative zones from 4 different mice were analyzed. Values were recorded in Microsoft Excel software, and the raw data was subsequently processed through Graphpad Prism software to conduct the statistical calculations and generate the graphical representations that show the data. Unpaired two-sample, two-tailed t-tests were used when comparing two groups. Two-way ANOVAs with the Tukey-Kramer test to account for multiple comparisons were used for comparisons of more than two groups.

Measurement and quantification of HCN1 intensity in basket cell projections. The difference in HCN1 fluorescence intensity between large and small pinceaux in control and

635 *Pcp2*^{Cre};*Slc32a1*$^{flox/flox}$ mutant tissues were analyzed using ImageJ software. A total of 54 large
636 and small basket cell pinceaux from 16 different animals (6 C57BL/6J controls, 6 *Slc32a1*$^{flox/flox}$
637 controls, and 4 *Pcp2*^{Cre};*Slc32a1*$^{flox/flox}$ mutants) were analyzed for corrected total cell
638 fluorescence (CTCF) values. Each image was captured at 20x magnification, and analysis was
639 focused on lobules VII-IX where the different basket cell sizes are particularly clear and easily
640 tracked for analysis. CTCF values were calculated by subtracting the product of the area of the
641 ROI within each basket and the mean pixel value of the image background, from the summed
642 pixel values within the ROI (Integrated Density), defined and written as:
643
644 CTCF = (*Integrated Density)* – (Area of ROI × *Mean Background Fluorescence*)
645
646 The ROI that we selected for each basket cell was kept consistent within the image at 9 pixels or
647 1 μm^2, as this allowed for the ROI to be small enough to fit within every basket in the image.
648 Background fluorescence for each image was set to the pixel value of a 1 μm^2 region where there
649 appeared to be a lack of fluorescence. Values were recorded in Microsoft Excel software, and the
650 raw data was subsequently processed through Graphpad Prism software to conduct the statistical
651 calculations and to generate the graphical representations that show the data. Unpaired two-
652 sample, two-tailed t-tests were used when comparing two groups. Two-way ANOVA's with the
653 Tukey-Kramer test to account for multiple comparisons were used for comparisons that involved
654 more than two groups.
655
656
657

Figure legends

Figure 1: Basket cells are inhibitory interneurons in the cerebellar cortex that innervate Purkinje cells with a unique terminal called the pinceau. A, Left; schematic of sagittal tissue section through the mouse brain illustrating key connections between the cerebellum and other major brain regions. Right; magnified schematic, depicted as a 3-dimensional image, of the cerebellar cortex showing the main cell types including Purkinje cells (green), granule cells (purple), and basket and stellate cells (red). Purkinje cell somata are contained in the Purkinje cell layer (PCL) underneath the molecular layer (ML), and directly below the Purkinje cell layer lies the granular layer (GL) containing granule cells and various classes of interneurons (blue). (+) and (–) indicate excitatory and inhibitory synapses, respectively. Known orientations of projections and cell morphologies are presented in both the sagittal ((A) anterior, (P) posterior) and coronal ((M) medial, (L) lateral) planes. **B**, Left; schematic of a Purkinje cell (PC, green) with an innervating basket cell (BC, red). Right; Golgi-Cox staining reveals the intricate innervation of basket cell axons onto the Purkinje cell soma and the axon initial segment (AIS). The ascending collaterals are not easily appreciated here. Basket cell axons initially form branching contacts on the somata of Purkinje cells, creating a basket-like shape (left bracket). Upon reaching the AIS, the axons extend terminal branches that converge to form the pinceau (right bracket). Scale bar is 15 μm. **C**, Coronal-cut cerebellar tissue sections from an adult mouse stained for HCN1, which reveals the zonal patterning of basket cell pinceau projections. Dotted lines indicate zone boundaries. Purkinje cell layer, molecular layer, and granular layer are indicated by PCL, ML, and GL, respectively. Basket cell pinceaux are located in the most superficial regions of the granular layer (GL). Scale bar is 100 μm.

Figure 2: HCN1-labeled basket cell pinceaux are smaller in zebrinII-positive zones and larger in zebrinII-negative Purkinje cell zones. A, **C, E**, Coronal section cut through the cerebellar cortex showing zebrinII (green, PC) and HCN1 (red, pinceau) expression. Dotted lines delineate the Purkinje cell zonal boundaries. Purkinje cell bodies are contained within the Purkinje cell layer (PCL) underneath the molecular layer (ML), and basket cell pinceaux are located in the superficial granular layer (GL) and PCL. **B**, **D, F**, Magnified image of a zebrinII zonal boundary from panel **A, C,** and **E**, respectively (left, zebrinII-negative; right, zebrinII-positive). **E**, **F**, Merged zebrinII and HCN1 expression patterns from **A**-**D**. Scale bars are 100 µm and 30 µm, respectively. Brackets in **F** highlight the pinceau size difference across a zebrinII Purkinje cell zonal boundary. **G**, Schematic depiction of pinceau size distinctions in zebrinII-positive and -negative zones. **H**, Whole-mount schematic diagram of the cerebellum showing the zebrinII expression pattern in lobule VIII. ZebrinII-positive zones in green are marked as P1+, P2+, and P3+ using the standard zebrinII zone nomenclature (see Sillitoe and Hawkes, 2002). **I**, Quantification of pinceau area across zebrinII Purkinje cell zones in C57BL/6J mice reveals significantly smaller total pinceau size in zebrinII-positive zones (mean = 131.4µm², SD = 44.76µm²) compared to negative zones (mean = 383.5µm², SD = 87.19µm²). Each data point indicates the total area of multiple HCN1-labeled pinceaux within a 100 µm-wide region of a zebrinII-positive or -negative Purkinje cell zone, reported in µm² (N = 6, n = 12 sections, 26 zebrinII-positive Purkinje cell zones and 26 zebrinII-negative Purkinje cell zones; ****p < 0.0001). **J**, Corrected total cell fluorescence (CTCF) analysis reveals no significant difference in HCN1-labeled pinceau fluorescence intensity between pinceaux associated with zebrinII-positive (mean = 73.9, SD = 3.3) and zebrinII-negative (mean = 73.41, SD = 3.55) Purkinje cells. Each data point represents the CTCF value of a 1µm² region in a single pinceau (N = 6 mice, n = 12

large and 12 small pinceaux; $p > 0.05$; note however, that although 6 mice were used for the quantitative analysis, the patterned relationship between HCN1 and zebrinII was consistently observed in every mouse studied so far, $N > 20$).

Figure 3: HCN1-labeled basket cell pinceaux are larger in PLCβ4-positive Purkinje cell zones. A, **C, E**, Coronal section cut through the cerebellar cortex showing PLCβ4 (green, PC) and HCN1 (red, pinceau) expression. Dotted lines indicate Purkinje cell zonal boundaries. Purkinje cell somata are contained within the Purkinje cell layer (PCL) underneath the molecular layer (ML), and basket cell pinceaux are observed in the granular layer (GL) and occasionally in the PCL. **B**, **D, F**, Higher magnification view of a PLCβ4 zonal boundary (left, PLCβ4-positive; right, PLCβ4-negative). Scale bars are 100 μm and 30 μm, respectively. Brackets in **F** highlight the pinceau size difference across a PLCβ4 Purkinje cell zonal boundary. **G**, Schematic depiction of the pinceau size differences in PLCβ4-positive and -negative zones. **H**, Whole-mount schematic diagram of the cerebellum showing the PLCβ4 and HCN1 expression patterns in lobule VIII. PLCβ4-positive zones in green are marked as P1- and P2- using the standard zebrinII zone nomenclature (Ozol et al., 1999; Sillitoe and Hawkes, 2002). Differences in HCN1-labeled pinceau sizes across PLCβ4 zones are labeled in dark red and light red, with larger pinceaux (dark red) located on Purkinje cells within the PLCβ4-positve zones ($N = 4$).

Figure 4: HCN1-labeled basket cell pinceaux are larger in NFH-positive Purkinje cell zones across different cerebellar lobules. A, **D**, **G**, Whole-mount cerebellum schematic showing NFH expression patterns in lobules VII, VIII, and IX respectively. NFH-positive zones are marked as 1, 2, 3. **B**, **C**, Coronal section cut through lobule VII showing NFH (green, Purkinje

727 cell) and HCN1 (red, pinceau) expression. Dotted lines delineate the Purkinje cell zonal
728 boundaries. The Purkinje cell layer (PCL), molecular layer (ML), and granular layer (GL) are
729 labeled as guides for locating the basket cell pinceaux. **E**, **F**, Coronal section cut through lobule
730 VIII showing NFH and HCN1 expression. **H**, **I**, Coronal section showing NFH and HCN1
731 expression in lobule IX. Scale bar is 100 μm. **J**, Schematic depiction of pinceau size differences
732 between NFH-positive (left) and -negative (right) zones, with larger pinceaux located on
733 Purkinje cells in the NFH-positive zones. Inset in the bottom left corner shows the difference
734 between pinceau sizes in an NFH-positive (left) and -negative (right) zone, in tissue from lobule
735 VIII stained with NFH (green) and HCN1 (red). Scale bar is 30 μm (*N* = 4).
736
737 **Figure 5: KV1.1, PSD95, and GAD67 are co-expressed with HCN1 in basket cell pinceaux.**
738 **A**, **B**, KV1.1 (green) and HCN1 (red) expression are located in the same pinceaux. **C**, Merged
739 KV1.1 and HCN1 signal. Scale bar is 60 μm (*N* = 7). **D**, **E**, **F**, Magnified images from dotted
740 square region indicated in **A** from **A**, **B**, **C** respectively, showing that KV1.1 and HCN1 immuno
741 signals are equally strong throughout the pinceaux. Scale bar in **F** is 20 μm. **G**, **H**, PSD95
742 (green) and HCN1 (red) expression are located in the same pinceaux. **I**, Merged PSD95 and
743 HCN1 signal. Scale bar is 60 μm. **J**, **K**, **L**, Magnified images from **G**, **H**, **I** respectively, showing
744 that PSD95 and HCN1 expression are equally strong throughout the pinceaux. Scale bar in **L** is
745 20 μm (*N* = 7). **M**, **N**, GAD67 (green) and HCN1 (red) expression are located in the same
746 pinceaux. **O**, Merged GAD67 and HCN1 signal. Scale bar is 60 μm. **P**, **Q**, **R**, Magnified images
747 from **M**, **N**, **O** respectively, showing that GAD67 and HCN1 expression are equally strong
748 throughout the pinceaux. Scale bar in **R** is 20 μm (*N* = 7).
749

Figure 6: KV1.1, PSD95, and GAD67 label basket cell pinceaux and adhere to the same zonal patterning as HCN1. A, Schematic of basket cell pinceau size differences across zonal boundaries. Dotted area around Purkinje cell somata depicts the boundary between a zebrinII-negative zone (left) and a zebrinII-positive zone (right). Basket cell pinceaux are larger, on average, in the zebrinII-negative zones. **B**, Magnified images of KV1.1, PSD95, GAD67 (green), and HCN1 (red) expression in basket cell pinceaux across a zebrinII zonal boundary. Dotted white lines indicate the boundary between a zebrinII-negative zone (left) and a zebrinII-positive zone (right). Pinceau sizes are distinctly larger in the zebrinII-negative zone as marked by all 4 pinceau markers. Merged HCN1 and KV1.1, PSD95, GAD67 expression is shown in the bottom row, respectively **(***N* = 7 for KV1.1, 7 for PSD95, and 7 for GAD67). Scale bars are 15 μm.

Figure 7: Genetically marked basket cell pinceaux are distinguished by size according to Purkinje cell zones. A, **B**, **C**, Coronal section cut through the cerebellar cortex showing IP3R1 (blue, PC), GFP (green, pinceau), and PLCβ4 (red, PC) expression in *Ascl1*^{CreERT2};*Tau*$^{flox\text{-}stop\text{-}mGFP\text{-}lacZ}$ tissue. Dotted line indicates the Purkinje cell boundary between a PLCβ4-positive (left) and PLCβ4-negative (right) zone. Scale bar in **A** is 50 μm. **D**, Merged IP3R1, GFP, and PLCβ4 expression. Brackets highlight genetically labeled-pinceaux of different sizes between PLCβ4-positive and -negative zones, which is consistent with the results from the HCN1-labeled pinceaux. **E**, Schematic of experimental timeline and procedure to generate genetically-labeled basket cells and pinceaux. Upon tamoxifen administration, the CreER protein that was sequestered in the cytoplasm by HSP is now able to enter the nucleus and induce recombination at *loxP* sites. Neurons are marked with GFP after recombination. **F**, Quantification of pinceau area across PLCβ4 zones reveals significantly higher total pinceau size in PLCβ4-positive zones

(mean = 537.7µm², SD = 125.2µm²) compared to PLCβ4-negative zones (mean = 166.5µm², SD = 62.17µm²). Each data point indicates the total area of multiple HCN1-labeled pinceaux within a 100 µm-wide region of a PLCβ4-positive or -negative Purkinje cell zone, in µm² (N = 4, n = 8 sections, 20 PLCβ4-positive zones and 22 PLCβ4-negative zones; ****$p < 0.0001$).

Figure 8: Zonal patterning of basket cell pinceaux is disrupted in *Pcp2^{Cre};Slc32a1$^{flox/flox}$* mutants. **A**, **B**, **C**, **D**, Anatomically matched coronal sections through lobule VIII showing zebrinII (green, PC) and HCN1 (red, pinceau) expression. **A**, **C**, *Slc32a1$^{flox/flox}$* (control) data. **B**, **D**, *Pcp2^{Cre};Slc32a1$^{flox/flox}$* (mutant) data, showing altered zonal organization of both Purkinje cells and pinceaux compared to controls. **E**, **F**, merged zebrinII and HCN1 expression in controls and mutants, respectively. Scale bar is 100 µm. **G**, Schematic whole-mount cerebellum diagram showing differences in pinceau size organization in *Slc32a1$^{flox/flox}$* controls and *Pcp2^{Cre};Slc32a1$^{flox/flox}$* mutants. In controls, pinceau sizes fall into distinct zonal domains, with dark red depicting areas with larger pinceaux and light red depicting those with smaller pinceaux. In the mutants, the zonal size organization is largely eliminated and across all regions. **H**, Left: quantification of pinceau area across Purkinje cell zones reveals significantly smaller total pinceau size in zebrinII-positive zones (mean = 124.8µm², SD = 45.65µm²) compared to zebrinII-negative zones (mean = 482.6µm², SD = 128.8µm²; $p < 0.0001$) in *Slc32a1$^{flox/flox}$* controls, but there was no significant difference in pinceau sizes in *Pcp2^{Cre};Slc32a1$^{flox/flox}$* mutants (mean = 166.5µm², SD = 71.94µm² for zebrinII-positive zones; mean = 178.7µm², SD = 81.72µm² for zebrinII-negative zones; $p = 0.9719$). Additionally, while both mutant zones had significantly smaller pinceaux compared to control zebrinII-negative zones (control zebrinII-negative vs. mutant zebrinII-positive $p < 0.0001$; control zebrinII-negative vs. mutant zebrinII-

796 negative $p < 0.0001$) there was no significant difference in the size of pinceaux between that of
797 the mutant zones and the size of pinceaux in the control zebrinII-positive zones (control zebrinII-
798 positive vs. mutant zebrinII-positive $p = 0.3883$; control zebrinII-positive vs. mutant zebrinII-
799 negative $p = 0.1755$). Each data point indicates the total area of the ROI covered by HCN1-
800 labeled pinceaux within a 100 µm-wide region of a zebrinII-positive or -negative Purkinje cell
801 zone, in µm². For mutant mice, $N = 4$, $n = 8$ sections, 20 zebrinII-positive Purkinje cell zones and
802 20 zebrinII-negative Purkinje cell zones. For controls, $N = 6$ mice, 12 sections, 26 zebrinII-
803 positive zones and 25 zebrinII-negative zones. Right: corrected total cell fluorescence (CTCF)
804 analysis reveals no significant difference in HCN1-labeled pinceau fluorescence intensity
805 between pinceaux associated with zebrinII-positive (mean = 72.24, SD = 7.22) and zebrinII-
806 negative (mean = 72.15, SD = 7.2) Purkinje cells, from both control and mutant animals. Each
807 data point represents the CTCF value of a 1µm² region in a single pinceau ($N = 6$ control and 4
808 mutant mice, $n = 18$ large and 18 small pinceaux; $p > 0.05$)
809
810 **Figure 9: Silencing basket cell GABAergic inhibitory neurotransmission does not affect the**
811 **zonal patterning of Purkinje cells. A**, Schematic representation of normal zebrinII patterning
812 across the whole mouse cerebellum, seen in a whole-mount configuration. **B**, Sagittal schematic
813 of a mouse cerebellum slice at the midline; the red vertical line indicates the anatomical location
814 of the coronal sections shown in **C** and **D**. The red dotted line indicates the location of the
815 cerebellum that the insets were acquired from. **C**, Coronal section from a control mouse given
816 tamoxifen at E18.5, stained to reveal normal zebrinII expression patterning ($N = 4$, scale bar is
817 500 µm). Because the *Ascl1*^{CreERT2} allele was not expressed in this animal, inhibitory
818 neurotransmission of basket cells was not affected. Inset in the top right corner shows a higher

power magnification image from Lobule III and IV/V in the anterior cerebellum (scale bar is 250 μm), with normal zebrinII zonal patterning for that region of the cerebellum. Coronal-cut tissue section from a mouse expressing both the *Ascl1*^{CreERT2} and *Slc32a1*$^{flox/flox}$ alleles, given tamoxifen at E18.5 to target the silencing of neurotransmission in basket cells. Because both the *Ascl1*^{CreERT2} and the *Slc32a1*$^{flox/flox}$ allele, which is used to delete *Slc32a1* with spatial and temporal control, were expressed in this animal, cerebellar basket cell neurotransmission was silenced throughout its lifetime. Despite this, staining in the anterior (top right inset), central and posterior lobules reveals that zebrinII patterning is unchanged in the absence of basket cell neurotransmission, as shown in **D** (N = 4). In lobule III and IV/V of the anterior cerebellum (inset), the ~500 μm distance between the P1+ and P2+ zebrinII zones (Sillitoe and Hawkes, 2002; Sillitoe et al., 2008b) and the sharpness of the zebrinII Purkinje cell zonal boundaries is maintained after GABAergic neurotransmission is genetically blocked at the basket cell terminals (scale bar is 250 μm).

Figure 2 – Figure Supplement 1: Sample antibody staining controls for the expression of protein markers in basket cell zones. A, **C**, **E**, Secondary antibody staining without the application of a primary antibody shows only the expected background, non-specific signal that is typical for Alexa 488 (green), Alexa 555 (red), and merged images, respectively. **B**, **D**, **F**, Primary antibody staining without the application of secondary antibody also shows the lack of an immunopositive signal for zebrinII (green), HCN1 (red) and merged images, respectively. Scale bar in **F** is 100 μm. **A**, **B**, were imaged to visualize the Alexa 488 fluorophore; **C**, **D**, were imaged to visualize the Alexa 555 fluorophore (N = 7).

Figure 2 – Figure Supplement 2: HCN1 expression reveals zones in the hemisphere lobules. **Top**, whole-mount schematic representation of zebrinII zonal expression (grey denotes positive domains) throughout the cerebellum. **A** – **D**, Coronal sections from hemispheric regions of the cerebellum showing HCN1 expression, visualized with DAB. Boxes **A** – **D** on the schematic correspond to the hemispheric regions depicted in images **A** – **D**, from Crus1, Crus2, paramedian, and copula pyramidis lobules. Dotted black lines indicate the boundaries between regions containing stronger HCN1 expression (corresponding to zebrinII-negative zones) and lower HCN1 expression (corresponding to zebrinII-positive zones). Scale bar in A is 50 μm (*N* = 6). The distinction between pinceau zones in the hemispheres is weak compared to the vermis.

Figure 7 – Figure Supplement 1: Controls for assessing genetically labeled basket cells. A, **B**, Coronal sections from two different animals that only have the *Tau*$^{flox\text{-}stop\text{-}mGFP\text{-}lacZ}$ allele and not the *Ascl1*^{CreERT2} allele. Staining with an Alexa 488 (green) secondary antibody shows that basket cells and their pinceaux are not genetically labeled with the myristoylated GFP without recombination using *Ascl1*^{CreERT2}. **C** and **D** show HCN1 (red) expression in basket cell pinceaux in the same tissue sections in **A** and **B**, respectively. **E**, **F**, Merged Alexa 488 (green) and HCN1 (red) expression from **A** – **D**. Scale bar in **F** is 50 μm (*N* = 3).

865 **References**

866 Ahn, A. H., Dziennis, S., Hawkes, R., & Herrup, K. (1994). The cloning of zebrin II reveals its
867 identity with aldolase C. *Development*, *120*(8), 2081–2090.

868 Alcami, P., & Marty, A. (2013). Estimating functional connectivity in an electrically coupled
869 interneuron network. *Proceedings of the National Academy of Sciences of the United States*
870 *of America*, *110*(49). https://doi.org/10.1073/pnas.1310983110

871 Ango, F., di Cristo, G., Higashiyama, H., Bennett, V., Wu, P., & Huang, Z. J. (2004). Ankyrin-
872 based subcellular gradient of neurofascin, an immunoglobulin family protein, directs
873 GABAergic innervation at purkinje axon initial segment. *Cell*, *119*(2), 257–272.
874 https://doi.org/10.1016/j.cell.2004.10.004

875 Apps, R., & Hawkes, R. (2009). Cerebellar cortical organization: a one-map hypothesis. *Nature*
876 *Reviews. Neuroscience*, *10*(9), 670–681. https://doi.org/10.1038/nrn2698

877 Apps, R., Hawkes, R., Aoki, S., Bengtsson, F., Brown, A. M., Chen, G., … Ruigrok, T. J. H.
878 (2018, October 1). Cerebellar Modules and Their Role as Operational Cerebellar Processing
879 Units. *Cerebellum*, Vol. 17, pp. 654–682. https://doi.org/10.1007/s12311-018-0952-3

880 Arimitsu, T., Nuriya, M., Ikeda, K., Takahashi, T., & Yasui, M. (2009). Activity-dependent
881 regulation of HCN1 protein in cortical neurons. *Biochemical and Biophysical Research*
882 *Communications*, *387*(1), 87–91. https://doi.org/10.1016/j.bbrc.2009.06.127

883 Armstrong, C. L., & Hawkes, R. (2000). Pattern formation in the cerebellar cortex. *Biochemistry*
884 *and Cell Biology = Biochimie et Biologie Cellulaire*, *78*(5), 551–562. Retrieved from
885 http://www.ncbi.nlm.nih.gov/pubmed/11103945

886 Attwell, P. J., Rahman, S., Ivarsson, M., & Yeo, C. H. (1999). Cerebellar cortical AMPA-kainate
887 receptor blockade prevents performance of classically conditioned nictitating membrane
888 responses. *The Journal of Neuroscience : The Official Journal of the Society for*
889 *Neuroscience*, *19*(24), RC45. Retrieved from
890 http://www.ncbi.nlm.nih.gov/pubmed/10594089

891 Attwell, P. J. E., Rahman, S., & Yeo, C. H. (2001). Acquisition of eyeblink conditioning is
892 critically dependent on normal function in cerebellar cortical lobule HVI. *Journal of*
893 *Neuroscience*, *21*(15), 5715–5722. https://doi.org/10.1523/jneurosci.21-15-05715.2001

894 Baader, S. L., Vogel, M. W., Sanlioglu, S., Zhang, X., & Oberdick, J. (1999). Selective
895 disruption of “late onset” sagittal banding patterns by ectopic expression of Engrailed-2 in
896 cerebellar Purkinje cells. *Journal of Neuroscience*, *19*(13), 5370–5379.
897 https://doi.org/10.1523/jneurosci.19-13-05370.1999

Barmack, N. H., & Yakhnitsa, V. (2008). Functions of interneurons in mouse cerebellum. *The Journal of Neuroscience : The Official Journal of the Society for Neuroscience*, *28*(5), 1140–1152. https://doi.org/10.1523/JNEUROSCI.3942-07.2008

Blot, A., & Barbour, B. (2014). Ultra-rapid axon-axon ephaptic inhibition of cerebellar Purkinje cells by the pinceau. *Nature Neuroscience*, *17*(2), 289–295. https://doi.org/10.1038/nn.3624

Bowers, M., Eng, L., Lao, Z., Turnbull, R. K., Bao, X., Riedel, E., … Joyner, A. L. (2012). Limb anterior-posterior polarity integrates activator and repressor functions of GLI2 as well as GLI3. *Developmental Biology*, *370*(1), 110–124. https://doi.org/10.1016/j.ydbio.2012.07.017

Braz, J. M., Rico, B., & Basbaum, A. I. (2002). Transneuronal tracing of diverse CNS circuits by Cre-mediated induction of wheat germ agglutinin in transgenic mice. *Proceedings of the National Academy of Sciences of the United States of America*, *99*(23), 15148–15153. https://doi.org/10.1073/pnas.222546999

Brochu, G., Maler, L., & Hawkes, R. (1990). Zebrin II: A polypeptide antigen expressed selectively by purkinje cells reveals compartments in rat and fish cerebellum. *Journal of Comparative Neurology*, *291*(4), 538–552. https://doi.org/10.1002/cne.902910405

Brown, A. M., Arancillo, M., Lin, T., Catt, D. R., Zhou, J., Lackey, E. P., … Sillitoe, R. V. (2019). Molecular layer interneurons shape the spike activity of cerebellar Purkinje cells. *Scientific Reports*, *9*(1). https://doi.org/10.1038/s41598-018-38264-1

Buttermore, E. D., Piochon, C., Wallace, M. L., Philpot, B. D., Hansel, C., & Bhat, M. A. (2012). Pinceau organization in the cerebellum requires distinct functions of neurofascin in Purkinje and basket neurons during postnatal development. *The Journal of Neuroscience : The Official Journal of the Society for Neuroscience*, *32*(14), 4724–4742. https://doi.org/10.1523/JNEUROSCI.5602-11.2012

Cajal, S. R. y. (1911). *Histologie du système nerveux de l'homme & des vertébrés*. Retrieved from https://archive.org/details/histologiedusyst01ram/page/n8

Cerminara, N. L., & Apps, R. (2011). Behavioural significance of cerebellar modules. *Cerebellum (London, England)*, *10*(3), 484–494. https://doi.org/10.1007/s12311-010-0209-2

Cerminara, N. L., Lang, E. J., Sillitoe, R. V, & Apps, R. (2015). Redefining the cerebellar cortex as an assembly of non-uniform Purkinje cell microcircuits. *Nature Reviews. Neuroscience*, *16*(2), 79–93. https://doi.org/10.1038/nrn3886

Chang, X., Wang, J., Jiang, H., Shi, L., & Xie, J. (2019). Hyperpolarization-Activated Cyclic Nucleotide-Gated Channels: An Emerging Role in Neurodegenerative Diseases. *Frontiers in Molecular Neuroscience*, *12*. https://doi.org/10.3389/fnmol.2019.00141

933 Chan-Palay, V., & Palay, S. L. (1970). Interrelations of basket cell axons and climbing fibers in
934 the cerebellar cortex of the rat. *Zeitschrift Für Anatomie Und Entwicklungsgeschichte*,
935 *132*(3), 191–227. https://doi.org/10.1007/BF00523377

936 Chaudhry, F. A., Reimer, R. J., Bellocchio, E. E., Danbolt, N. C., Osen, K. K., Edwards, R. H.,
937 & Storm-Mathisen, J. (1998). The vesicular GABA transporter, VGAT, localizes to
938 synaptic vesicles in sets of glycinergic as well as GABAergic neurons. *Journal of*
939 *Neuroscience*, *18*(23), 9733–9750. https://doi.org/10.1523/jneurosci.18-23-09733.1998

940 Chung, S.-H., Sillitoe, R. V, Croci, L., Badaloni, A., Consalez, G., & Hawkes, R. (2009).
941 Purkinje cell phenotype restricts the distribution of unipolar brush cells. *Neuroscience*,
942 *164*(4), 1496–1508. https://doi.org/10.1016/j.neuroscience.2009.09.080

943 Croci, L., Chung, S. H., Masserdotti, G., Gianola, S., Bizzoca, A., Gennarini, G., … Consalez, G.
944 G. (2006). A key role for the HLH transcription factor EBF2COE2,O/E-3 in Purkinje
945 neuron migration and cerebellar cortical topography. *Development*, *133*(14), 2719–2729.
946 https://doi.org/10.1242/dev.02437

947 Demilly, A., Reeber, S. L., Gebre, S. A., & Sillitoe, R. V. (2011). Neurofilament heavy chain
948 expression reveals a unique parasagittal stripe topography in the mouse cerebellum.
949 *Cerebellum (London, England)*, *10*(3), 409–421. https://doi.org/10.1007/s12311-010-0156-
950 y

951 Fujii, M., Arata, A., Kanbara-Kume, N., Saito, K., Yanagawa, Y., & Obata, K. (2007).
952 Respiratory activity in brainstem of fetal mice lacking glutamate decarboxylase 65/67 and
953 vesicular GABA transporter. *Neuroscience*, *146*(3), 1044–1052.
954 https://doi.org/10.1016/j.neuroscience.2007.02.050

955 Fujita, H., Oh-Nishi, A., Obayashi, S., & Sugihara, I. (2010). Organization of the marmoset
956 cerebellum in three-dimensional space: Lobulation, aldolase c compartmentalization and
957 axonal projection. *Journal of Comparative Neurology*, *518*(10), 1764–1791.
958 https://doi.org/10.1002/cne.22301

959 Fukaya, M., Uchigashima, M., Nomura, S., Hasegawa, Y., Kikuchi, H., & Watanabe, M. (2008).
960 Predominant expression of phospholipase Cbeta1 in telencephalic principal neurons and
961 cerebellar interneurons, and its close association with related signaling molecules in
962 somatodendritic neuronal elements. *The European Journal of Neuroscience*, *28*(9), 1744–
963 1759. https://doi.org/10.1111/j.1460-9568.2008.06495.x

964 Fukaya, M., & Watanabe, M. (2000). Improved immunohistochemical detection of
965 postsynaptically located PSD-95/SAP90 protein family by protease section pretreatment: A
966 study in the adult mouse brainfile:///Users/Yuko 1/Desktop/Mendeley PDF/Fukaya_et_al-
967 2000-Journal_of_Comparative_Neurology.p. *Journal of Comparative Neurology*, *426*(4),
968 572–586. https://doi.org/10.1002/1096-9861(20001030)426:4<572::AID-CNE6>3.0.CO;2-
969 9

970 Furutama, D., Morita, N., Takano, R., Sekine, Y., Sadakata, T., Shinoda, Y., … Furuichi, T.
971 (2010). Expression of the IP3R1 promoter-driven nls-lacZ transgene in Purkinje cell
972 parasagittal arrays of developing mouse cerebellum. *Journal of Neuroscience Research*,
973 *88*(13), 2810–2825. https://doi.org/10.1002/jnr.22451

974 Gebre, S. A., Reeber, S. L., & Sillitoe, R. V. (2012). Parasagittal compartmentation of cerebellar
975 mossy fibers as revealed by the patterned expression of vesicular glutamate transporters
976 VGLUT1 and VGLUT2. *Brain Structure & Function*, *217*(2), 165–180.
977 https://doi.org/10.1007/s00429-011-0339-4

978 Giacomo Consalez, G., & Hawkes, R. (2013, January 22). The compartmental restriction of
979 cerebellar interneurons. *Frontiers in Neural Circuits*.
980 https://doi.org/10.3389/fncir.2012.00123

981 Graham, D. J., & Wylie, D. R. (2012). Zebrin-immunopositive and -immunonegative stripe pairs
982 represent functional units in the pigeon vestibulocerebellum. *The Journal of*
983 *Neuroscience : The Official Journal of the Society for Neuroscience*, *32*(37), 12769–
984 12779. https://doi.org/10.1523/JNEUROSCI.0197-12.2012

985 Gravel, C., Eisenman, L. M., Sasseville, R., & Hawkes, R. (1987). Parasagittal organization of
986 the rat cerebellar cortex: direct correlation between antigenic Purkinje cell bands revealed
987 by mabQ113 and the organization of the olivocerebellar projection. *The Journal of*
988 *Comparative Neurology*, *265*(2), 294–310. https://doi.org/10.1002/cne.902650211

989 Grosse, G., Draguhn, A., Höhne, L., Tapp, R., Veh, R. W., & Ahnert-Hilger, G. (2000).
990 Expression of Kv1 potassium channels in mouse hippocampal primary cultures:
991 Development and activity-dependent regulation. *Journal of Neuroscience*, *20*(5), 1869–
992 1882. https://doi.org/10.1523/jneurosci.20-05-01869.2000

993 Hámori, J., & Szentágothai, J. (1965). The Purkinje cell baskets: ultrastructure of an inhibitory
994 synapse. *Acta Biologica Academiae Scientiarum Hungaricae*, *15*(4), 465–479. Retrieved
995 from http://www.ncbi.nlm.nih.gov/pubmed/5837132

996 Hantman, A. W., & Jessell, T. M. (2010). Clarke's column neurons as the focus of a
997 corticospinal corollary circuit. *Nature Neuroscience*, *13*(10), 1233–1239.
998 https://doi.org/10.1038/nn.2637

999 Hashimoto, M., & Mikoshiba, K. (2003). Mediolateral Compartmentalization of the Cerebellum
1000 Is Determined on the "Birth Date" of Purkinje Cells. *Journal of Neuroscience*, *23*(36),
1001 11342–11351. https://doi.org/10.1523/jneurosci.23-36-11342.2003

1002 Hashimoto, M., & Mikoshiba, K. (2003). Mediolateral Compartmentalization of the Cerebellum
1003 Is Determined on the "Birth Date" of Purkinje Cells. *Journal of Neuroscience*, *23*(36),
1004 11342–11351. https://doi.org/10.1523/jneurosci.23-36-11342.2003

1005 Hawkes, R. (1997). An anatomical model of cerebellar modules. *Progress in Brain Research*,
1006 Vol. 114, pp. 39–54. https://doi.org/10.1016/s0079-6123(08)63357-9

1007 Hawkes, R., & Leclerc, N. (1987). Antigenic map of the rat cerebellar cortex: the distribution of
1008 parasagittal bands as revealed by monoclonal anti-Purkinje cell antibody mabQ113. *The*
1009 *Journal of Comparative Neurology*, *256*(1), 29–41. https://doi.org/10.1002/cne.902560104

1010 He, C., Chen, F., Li, B., & Hu, Z. (2014). Neurophysiology of HCN channels: from cellular
1011 functions to multiple regulations. *Progress in Neurobiology*, *112*, 1–23.
1012 https://doi.org/10.1016/j.pneurobio.2013.10.001

1013 Heiney, S. A., Wohl, M. P., Chettih, S. N., Ruffolo, L. I., & Medina, J. F. (2014). Cerebellar-
1014 dependent expression of motor learning during eyeblink conditioning in head-fixed mice.
1015 *Journal of Neuroscience*, *34*(45), 14845–14853. https://doi.org/10.1523/JNEUROSCI.2820-
1016 14.2014

1017 Hippenmeyer, S., Vrieseling, E., Sigrist, M., Portmann, T., Laengle, C., Ladle, D. R., & Arber, S.
1018 (2005). A developmental switch in the response of DRG neurons to ETS transcription factor
1019 signaling. *PLoS Biology*, *3*(5), 0878–0890. https://doi.org/10.1371/journal.pbio.0030159

1020 Horn, K. M., Pong, M., & Gibson, A. R. (2010). Functional relations of cerebellar modules of
1021 the cat. *Journal of Neuroscience*, *30*(28), 9411–9423.
1022 https://doi.org/10.1523/JNEUROSCI.0440-10.2010

1023 Iwakura, A., Uchigashima, M., Miyazaki, T., Yamasaki, M., & Watanabe, M. (2012). Lack of
1024 molecular-anatomical evidence for GABAergic influence on axon initial segment of
1025 cerebellar Purkinje cells by the pinceau formation. *Journal of Neuroscience*, *32*(27), 9438–
1026 9448. https://doi.org/10.1523/JNEUROSCI.1651-12.2012

1027 Kano, M., & Watanabe, T. (2019). Developmental synapse remodeling in the cerebellum and
1028 visual thalamus. *F1000Research*, *8*, 1191. https://doi.org/10.12688/f1000research.18903.1

1029 Kistner, U., Wenzel, B. M., Veh, R. W., Cases-Langhoff, C., Garner, A. M., Appeltauer, U., …
1030 Garner, C. C. (1993). SAP90, a rat presynaptic protein related to the product of the
1031 Drosophila tumor suppressor gene dlg-A. *The Journal of Biological Chemistry*, *268*(7),
1032 4580–4583. Retrieved from http://www.ncbi.nlm.nih.gov/pubmed/7680343

1033 Korn, H., & Axelrad, H. (1980). Electrical inhibition of Purkinje cells in the cerebellum of the
1034 rat. *Proceedings of the National Academy of Sciences of the United States of America*,
1035 *77*(10), 6244–6247. https://doi.org/10.1073/pnas.77.10.6244

1036 Larouche, M., Beffert, U., Herz, J., & Hawkes, R. (2008). The Reelin receptors Apoer2 and
1037 Vldlr coordinate the patterning of Purkinje cell topography in the developing mouse
1038 cerebellum. *PloS One*, *3*(2), e1653. https://doi.org/10.1371/journal.pone.0001653

1039 Laube, G., Röper, J., Pitt, J. C., Sewing, S., Kistner, U., Garner, C. C., … Veh, R. W. (1996).
1040 Ultrastructural localization of Shaker-related potassium channel subunits and synapse-
1041 associated protein 90 to septate-like junctions in rat cerebellar Pinceaux. *Brain Research. Molecular Brain Research*, *42*(1), 51–61. https://doi.org/10.1016/s0169-328x(96)00120-9

1043 Lee, K. H., Mathews, P. J., Reeves, A. M. B., Choe, K. Y., Jami, S. A., Serrano, R. E., & Otis, T.
1044 S. (2015). Circuit mechanisms underlying motor memory formation in the cerebellum.
1045 *Neuron*, *86*(2), 529–540. https://doi.org/10.1016/j.neuron.2015.03.010

1046 Lewis, P. M., Gritli-Linde, A., Smeyne, R., Kottmann, A., & McMahon, A. P. (2004). Sonic
1047 hedgehog signaling is required for expansion of granule neuron precursors and patterning of
1048 the mouse cerebellum. *Developmental Biology*, *270*(2), 393–410.
1049 https://doi.org/10.1016/j.ydbio.2004.03.007

1050 Long, R. M., Pakan, J. M. P., Graham, D. J., Hurd, P. L., Gutierrez-Ibañez, C., & Wylie, D. R.
1051 (2018). Modulation of complex spike activity differs between zebrin-positive and -negative
1052 Purkinje cells in the pigeon cerebellum. *Journal of Neurophysiology*, *120*(1), 250–262.
1053 https://doi.org/10.1152/jn.00797.2017

1054 Lu, Y., Monsivais, P., Tempel, B. L., & Rubel, E. W. (2004). Activity-Dependent Regulation of
1055 the Potassium Channel Subunits Kv1.1 and Kv3.1. *Journal of Comparative Neurology*,
1056 *470*(1), 93–106. https://doi.org/10.1002/cne.11037

1057 Luján, R., Albasanz, J. L., Shigemoto, R., & Juiz, J. M. (2005). Preferential localization of the
1058 hyperpolarization-activated cyclic nucleotide-gated cation channel subunit HCN1 in basket
1059 cell terminals of the rat cerebellum. *The European Journal of Neuroscience*, *21*(8), 2073–
1060 2082. https://doi.org/10.1111/j.1460-9568.2005.04043.x

1061 McIntire, S. L., Reimer, R. J., Schuske, K., Edwards, R. H., & Jorgensen, E. M. (1997).
1062 Identification and characterization of the vesicular GABA transporter. *Nature*, *389*(6653),
1063 870–876. https://doi.org/10.1038/39908

1064 Millen, K. J., Hui, C. C., & Joyner, A. L. (1995). A role for En-2 and other murine homologues
1065 of Drosophila segment polarity genes in regulating positional information in the developing
1066 cerebellum. *Development*, *121*(12).

1067 Miterko, L. N., Lackey, E. P., Heck, D. H., & Sillitoe, R. V. (2018, October 10). Shaping
1068 Diversity Into the Brain's Form and Function. *Frontiers in Neural Circuits*, Vol. 12.
1069 https://doi.org/10.3389/fncir.2018.00083

1070 Moosmang, S., Biel, M., Hofmann, F., & Ludwig, A. (1999). Differential distribution of four
1071 hyperpolarization-activated cation channels in mouse brain. *Biological Chemistry*, *380*(7–
1072 8), 975–980. https://doi.org/10.1515/BC.1999.121

1073 Moosmang, S., Stieber, J., Zong, X., Biel, M., Hofmann, F., & Ludwig, A. (2001). Cellular
1074 expression and functional characterization of four hyperpolarization-activated pacemaker

channels in cardiac and neuronal tissues. *European Journal of Biochemistry*, *268*(6), 1646–1652. https://doi.org/10.1046/j.1432-1327.2001.02036.x

Mostofi, A., Holtzman, T., Grout, A. S., Yeo, C. H., & Edgley, S. A. (2010). Electrophysiological localization of eyeblink-related microzones in rabbit cerebellar cortex. *Journal of Neuroscience*, *30*(26), 8920–8934. https://doi.org/10.1523/JNEUROSCI.6117-09.2010

Nakayama, H., Miyazaki, T., Kitamura, K., Hashimoto, K., Yanagawa, Y., Obata, K., … Kano, M. (2012). GABAergic Inhibition Regulates Developmental Synapse Elimination in the Cerebellum. *Neuron*, *74*(2), 384–396. https://doi.org/10.1016/j.neuron.2012.02.032

Namba, K., Sugihara, I., & Hashimoto, M. (2011). Close correlation between the birth date of Purkinje cells and the longitudinal compartmentalization of the mouse adult cerebellum. *The Journal of Comparative Neurology*, *519*(13), 2594–2614. https://doi.org/10.1002/cne.22640

Nolan, M. F., Malleret, G., Lee, K. H., Gibbs, E., Dudman, J. T., Santoro, B., … Morozov, A. (2003). The hyperpolarization-activated HCN1 channel is important for motor learning and neuronal integration by cerebellar Purkinje cells. *Cell*, *115*(5), 551–564. https://doi.org/10.1016/s0092-8674(03)00884-5

Notomi, T., & Shigemoto, R. (2004). Immunohistochemical localization of Ih channel subunits, HCN1-4, in the rat brain. *The Journal of Comparative Neurology*, *471*(3), 241–276. https://doi.org/10.1002/cne.11039

Ozol, K., Hayden, J. M., Oberdick, J., & Hawkes, R. (1999). Transverse zones in the vermis of the mouse cerebellum. *Journal of Comparative Neurology*, *412*(1), 95–111. https://doi.org/10.1002/(SICI)1096-9861(19990913)412:1<95::AID-CNE7>3.0.CO;2-Y

Pakan, J. M. P., Graham, D. J., & Wylie, D. R. (2010). Organization of visual mossy fiber projections and zebrin expression in the pigeon vestibulocerebellum. *Journal of Comparative Neurology*, *518*(2), 175–198. https://doi.org/10.1002/cne.22192

Palay, S. L., & Chan-Palay, V. (1974). *Cerebellar cortex: cytology and organization*. Springer.

Paukert, M., Huang, Y. H., Tanaka, K., Rothstein, J. D., & Bergles, D. E. (2010). Zones of enhanced glutamate release from climbing fibers in the mammalian cerebellum. *Journal of Neuroscience*, *30*(21), 7290–7299. https://doi.org/10.1523/JNEUROSCI.5118-09.2010

Pijpers, A., & Ruigrok, T. J. H. (2006). Organization of pontocerebellar projections to identified climbing fiber zones in the rat. *The Journal of Comparative Neurology*, *496*(4), 513–528. https://doi.org/10.1002/cne.20940

Quy, P. N., Fujita, H., Sakamoto, Y., Na, J., & Sugihara, I. (2011). Projection patterns of single mossy fiber axons originating from the dorsal column nuclei mapped on the aldolase C

compartments in the rat cerebellar cortex. *The Journal of Comparative Neurology*, *519*(5), 874–899. https://doi.org/10.1002/cne.22555

Reeber, S. L., Arancillo, M., & Sillitoe, R. V. (2018). Bergmann Glia are Patterned into Topographic Molecular Zones in the Developing and Adult Mouse Cerebellum. *Cerebellum (London, England)*, *17*(4), 392–403. https://doi.org/10.1007/s12311-014-0571-6

Reeber, S. L., Otis, T. S., & Sillitoe, R. V. (2013). New roles for the cerebellum in health and disease. *Frontiers in Systems Neuroscience*, *7*, 83. https://doi.org/10.3389/fnsys.2013.00083

Reeber, S. L., & Sillitoe, R. V. (2011). Patterned expression of a cocaine- and amphetamine-regulated transcript peptide reveals complex circuit topography in the rodent cerebellar cortex. *The Journal of Comparative Neurology*, *519*(9), 1781–1796. https://doi.org/10.1002/cne.22601

Rieubland, S., Roth, A., & Häusser, M. (2014). Structured connectivity in cerebellar inhibitory networks. *Neuron*, *81*(4), 913–929. https://doi.org/10.1016/j.neuron.2013.12.029

Roberts, T. D. M. (1968). THE CEREBELLUM AS A NEURONAL MACHINE. By John C. Eccles, Masao Ito and János Szentágothai. Berlin, Heidelberg, New York: Springer Verlag. 1967. Pp. 335. 62s. *Quarterly Journal of Experimental Physiology and Cognate Medical Sciences*, *53*(3), 337–338. https://doi.org/10.1113/expphysiol.1968.sp001975

Ruigrok, T. J. H. (2011). Ins and outs of cerebellar modules. *Cerebellum (London, England)*, *10*(3), 464–474. https://doi.org/10.1007/s12311-010-0164-y

Saito, K., Kakizaki, T., Hayashi, R., Nishimaru, H., Furukawa, T., Nakazato, Y., … Yanagawa, Y. (2010). The physiological roles of vesicular GABA transporter during embryonic development: a study using knockout mice. *Molecular Brain*, *3*, 40. https://doi.org/10.1186/1756-6606-3-40

Santoro, B., Grant, S. G. N., Bartsch, D., & Kandel, E. R. (1997). Interactive cloning with the SH3 domain of N-src identifies a new brain specific ion channel protein, with homology to Eag and cyclic nucleotide-gated channels. *Proceedings of the National Academy of Sciences of the United States of America*, *94*(26), 14815–14820. https://doi.org/10.1073/pnas.94.26.14815

Sarna, J. R., Marzban, H., Watanabe, M., & Hawkes, R. (2006). Complementary stripes of phospholipase Cbeta3 and Cbeta4 expression by Purkinje cell subsets in the mouse cerebellum. *The Journal of Comparative Neurology*, *496*(3), 303–313. https://doi.org/10.1002/cne.20912

Schindelin, J., Arganda-Carreras, I., Frise, E., Kaynig, V., Longair, M., Pietzsch, T., … Cardona, A. (2012, July). Fiji: An open-source platform for biological-image analysis. *Nature Methods*, Vol. 9, pp. 676–682. https://doi.org/10.1038/nmeth.2019

Schonewille, M., Luo, C., Ruigrok, T. J. H., Voogd, J., Schmolesky, M. T., Rutteman, M., … De Zeeuw, C. I. (2006). Zonal organization of the mouse flocculus: Physiology, input, and output. *Journal of Comparative Neurology*, *497*(4), 670–682. https://doi.org/10.1002/cne.21036

Sillitoe, R. V, Gopal, N., & Joyner, A. L. (2009). Embryonic origins of ZebrinII parasagittal stripes and establishment of topographic Purkinje cell projections. *Neuroscience*, *162*(3), 574–588. https://doi.org/10.1016/j.neuroscience.2008.12.025

Sillitoe, R. V., Benson, M. A., Blake, D. J., & Hawkes, R. (2003). Abnormal dysbindin expression in cerebellar mossy fiber synapses in the mdx mouse model of Duchenne muscular dystrophy. *Journal of Neuroscience*, *23*(16), 6576–6585. https://doi.org/10.1523/jneurosci.23-16-06576.2003

Sillitoe, R. V., Chung, S. H., Fritschy, J. M., Hoy, M., & Hawkes, R. (2008). Golgi cell dendrites are restricted by purkinje cell stripe boundaries in the adult mouse cerebellar cortex. *Journal of Neuroscience*, *28*(11), 2820–2826. https://doi.org/10.1523/JNEUROSCI.4145-07.2008

Sillitoe, R. V., Chung, S. H., Fritschy, J. M., Hoy, M., & Hawkes, R. (2008a). Golgi cell dendrites are restricted by purkinje cell stripe boundaries in the adult mouse cerebellar cortex. *Journal of Neuroscience*, *28*(11), 2820–2826. https://doi.org/10.1523/JNEUROSCI.4145-07.2008

Sillitoe, R. V., & Joyner, A. L. (2007). Morphology, Molecular Codes, and Circuitry Produce the Three-Dimensional Complexity of the Cerebellum. *Annual Review of Cell and Developmental Biology*, *23*(1), 549–577. https://doi.org/10.1146/annurev.cellbio.23.090506.123237

Sillitoe, R. V, & Hawkes, R. (2002). Whole-mount immunohistochemistry: a high-throughput screen for patterning defects in the mouse cerebellum. *The Journal of Histochemistry and Cytochemistry : Official Journal of the Histochemistry Society*, *50*(2), 235–244. https://doi.org/10.1177/002215540205000211

Sillitoe, R. V, Stephen, D., Lao, Z., & Joyner, A. L. (2008b). Engrailed homeobox genes determine the organization of Purkinje cell sagittal stripe gene expression in the adult cerebellum. *The Journal of Neuroscience : The Official Journal of the Society for Neuroscience*, *28*(47), 12150–12162. https://doi.org/10.1523/JNEUROSCI.2059-08.2008

Sillitoe, R. V, Vogel, M. W., & Joyner, A. L. (2010). Engrailed homeobox genes regulate establishment of the cerebellar afferent circuit map. *The Journal of Neuroscience : The Official Journal of the Society for Neuroscience*, *30*(30), 10015–10024. https://doi.org/10.1523/JNEUROSCI.0653-10.2010

Sivilia, S., Mangano, C., Beggiato, S., Giuliani, A., Torricella, R., Baldassarro, V. A., … Calzà, L. (2016). CDKL5 knockout leads to altered inhibitory transmission in the cerebellum of adult mice. *Genes, Brain and Behavior*, *15*(5), 491–502. https://doi.org/10.1111/gbb.12292

1183 Somogyu, P., & Hámori, J. (1976). A quantitative electron microscopic study of the purkinje cell
1184 axon initial segment. *Neuroscience*, *1*(5). https://doi.org/10.1016/0306-4522(76)90127-5

1185 Sotelo, C. (2008). Development of “Pinceaux” formations and dendritic translocation of
1186 climbing fibers during the acquisition of the balance between glutamatergic and gamma-
1187 aminobutyric acidergic inputs in developing Purkinje cells. *The Journal of Comparative*
1188 *Neurology*, *506*(2), 240–262. https://doi.org/10.1002/cne.21501

1189 Sotelo, C. (2015). Molecular layer interneurons of the cerebellum: developmental and
1190 morphological aspects. *Cerebellum (London, England)*, *14*(5), 534–556.
1191 https://doi.org/10.1007/s12311-015-0648-x

1192 Stay, T. L., Laurens, J., Sillitoe, R. V., & Angelaki, D. E. (2019). Genetically eliminating
1193 Purkinje neuron GABAergic neurotransmission increases their response gain to vestibular
1194 motion. *Proceedings of the National Academy of Sciences of the United States of America*,
1195 *116*(8), 3245–3250. https://doi.org/10.1073/pnas.1818819116

1196 Subramanian, J., Michel, K., Benoit, M., & Nedivi, E. (2019). CPG15/Neuritin Mimics
1197 Experience in Selecting Excitatory Synapses for Stabilization by Facilitating PSD95
1198 Recruitment. *Cell Reports*, *28*(6), 1584-1595.e5.
1199 https://doi.org/10.1016/j.celrep.2019.07.012

1200 Sudarov, A., Turnbull, R. K., Kim, E. J., Lebel-Potter, M., Guillemot, F., & Joyner, A. L. (2011).
1201 Ascl1 genetics reveals insights into cerebellum local circuit assembly. *The Journal of*
1202 *Neuroscience : The Official Journal of the Society for Neuroscience*, *31*(30), 11055–
1203 11069. https://doi.org/10.1523/JNEUROSCI.0479-11.2011

1204 Sugihara, I., & Quy, P. N. (2007). Identification of aldolase C compartments in the mouse
1205 cerebellar cortex by olivocerebellar labeling. *The Journal of Comparative Neurology*,
1206 *500*(6), 1076–1092. https://doi.org/10.1002/cne.21219

1207 Sugihara, I., & Shinoda, Y. (2007). Molecular, topographic, and functional organization of the
1208 cerebellar nuclei: analysis by three-dimensional mapping of the olivonuclear projection and
1209 aldolase C labeling. *The Journal of Neuroscience : The Official Journal of the Society for*
1210 *Neuroscience*, *27*(36), 9696–9710. https://doi.org/10.1523/JNEUROSCI.1579-07.2007

1211 Szapiro, G., & Barbour, B. (2007). Multiple climbing fibers signal to molecular layer
1212 interneurons exclusively via glutamate spillover. *Nature Neuroscience*, *10*(6), 735–742.
1213 https://doi.org/10.1038/nn1907

1214 Tang, T., Xiao, J., Suh, C. Y., Burroughs, A., Cerminara, N. L., Jia, L., … Lang, E. J. (2017).
1215 Heterogeneity of Purkinje cell simple spike–complex spike interactions: zebrin- and non-
1216 zebrin-related variations. *Journal of Physiology*, *595*(15), 5341–5357.
1217 https://doi.org/10.1113/JP274252

1218 Telley, L., Cadilhac, C., Cioni, J.-M., Saywell, V., Jahannault-Talignani, C., Huettl, R. E., …
1219 Ango, F. (2016). Dual Function of NRP1 in Axon Guidance and Subcellular Target
1220 Recognition in Cerebellum. *Neuron*, *91*(6), 1276–1291.
1221 https://doi.org/10.1016/j.neuron.2016.08.015

1222 Tolbert, D. L., Pittman, T., Alisky, J. M., & Clark, B. R. (1994). Chronic NMDA receptor
1223 blockade or muscimol inhibition of cerebellar cortical neuronal activity alters the
1224 development of spinocerebellar afferent topography. *Brain Research. Developmental Brain*
1225 *Research*, *80*(1–2), 268–274. https://doi.org/10.1016/0165-3806(94)90112-0

1226 Tong, Q., Ye, C.-P., Jones, J. E., Elmquist, J. K., & Lowell, B. B. (2008). Synaptic release of
1227 GABA by AgRP neurons is required for normal regulation of energy balance. *Nature*
1228 *Neuroscience*, *11*(9), 998–1000. https://doi.org/10.1038/nn.2167

1229 Voogd, J., Pardoe, J., Ruigrok, T. J. H., & Apps, R. (2003). The distribution of climbing and
1230 mossy fiber collateral branches from the copula pyramidis and the paramedian lobule:
1231 Congruence of climbing fiber cortical zones and the pattern of zebrin banding within the rat
1232 cerebellum. *Journal of Neuroscience*, *23*(11), 4645–4656.
1233 https://doi.org/10.1523/jneurosci.23-11-04645.2003

1234 Voogd, J., & Ruigrok, T. J. H. (2004). The organization of the corticonuclear and olivocerebellar
1235 climbing fiber projections to the rat cerebellar vermis: The congruence of projection zones
1236 and the zebrin pattern. *Journal of Neurocytology*, *33*(1 SPEC. ISS.), 5–21.
1237 https://doi.org/10.1023/B:NEUR.0000029645.72074.2b

1238 Voogd, J. (1964). The cerebellum of the cat: structure and fibre connexions. *FA Davis Co.*, *2*.

1239 Wadiche, J. I., & Jahr, C. E. (2005). Patterned expression of Purkinje cell glutamate transporters
1240 controls synaptic plasticity. *Nature Neuroscience*, *8*(10), 1329–1334.
1241 https://doi.org/10.1038/nn1539

1242 Wang, H., Kunkel, D. O., Schwartzkroin, P. A., & Tempel, B. L. (1994). Localization of Kv1.1
1243 and Kv1.2, two K channel proteins, to synaptic terminals, somata, and dendrites in the
1244 mouse brain. *Journal of Neuroscience*, *14*(8), 4588–4599.
1245 https://doi.org/10.1523/jneurosci.14-08-04588.1994

1246 Welsh, J. P., Lang, E. J., Sugihara, I., & Llinas, R. (1995). Dynamic organization of motor
1247 control within the olivocerebellar system. *Nature*, *374*(6521), 453–457.
1248 https://doi.org/10.1038/374453a0

1249 White, J. J., & Sillitoe, R. V. (2013). Postnatal development of cerebellar zones revealed by
1250 neurofilament heavy chain protein expression. *Frontiers in Neuroanatomy*, (APR).
1251 https://doi.org/10.3389/fnana.2013.00009

White, J. J., & Sillitoe, R. V. (2017). Genetic silencing of olivocerebellar synapses causes dystonia-like behaviour in mice. *Nature Communications*, *8*. https://doi.org/10.1038/ncomms14912

White, J. J., Arancillo, M., Stay, T. L., George-Jones, N. A., Levy, S. L., Heck, D. H., & Sillitoe, R. V. (2014). Cerebellar zonal patterning relies on Purkinje cell neurotransmission. *The Journal of Neuroscience: The Official Journal of the Society for Neuroscience*, *34*(24), 8231–8245. https://doi.org/10.1523/JNEUROSCI.0122-14.2014

Wu, B., Blot, F. G., Wong, A. B., Osório, C., Adolfs, Y., Pasterkamp, R. J., … Schonewille, M. (2019). TRPC3 is a major contributor to functional heterogeneity of cerebellar Purkinje cells. *ELife*, *8*. https://doi.org/10.7554/elife.45590

Xiao, J., Cerminara, N. L., Kotsurovskyy, Y., Aoki, H., Burroughs, A., Wise, A. K., … Lang, E. J. (2014). Systematic regional variations in Purkinje cell spiking patterns. *PLoS ONE*, *9*(8). https://doi.org/10.1371/journal.pone.0105633

Zervas, M., Millet, S., Ahn, S., & Joyner, A. L. (2004). Cell behaviors and genetic lineages of the mesencephalon and rhombomere 1. *Neuron*, *43*(3), 345–357. https://doi.org/10.1016/j.neuron.2004.07.010

Zhou, H., Lin, Z., Voges, K., Ju, C., Gao, Z., Bosman, L. W. J., … Schonewille, M. (2014). Cerebellar modules operate at different frequencies. *ELife*, *2014*(3). https://doi.org/10.7554/eLife.02536

Zonta, B., Desmazieres, A., Rinaldi, A., Tait, S., Sherman, D. L., Nolan, M. F., & Brophy, P. J. (2011). A Critical Role for Neurofascin in Regulating Action Potential Initiation through Maintenance of the Axon Initial Segment. *Neuron*, *69*(5), 945–956. https://doi.org/10.1016/j.neuron.2011.02.021

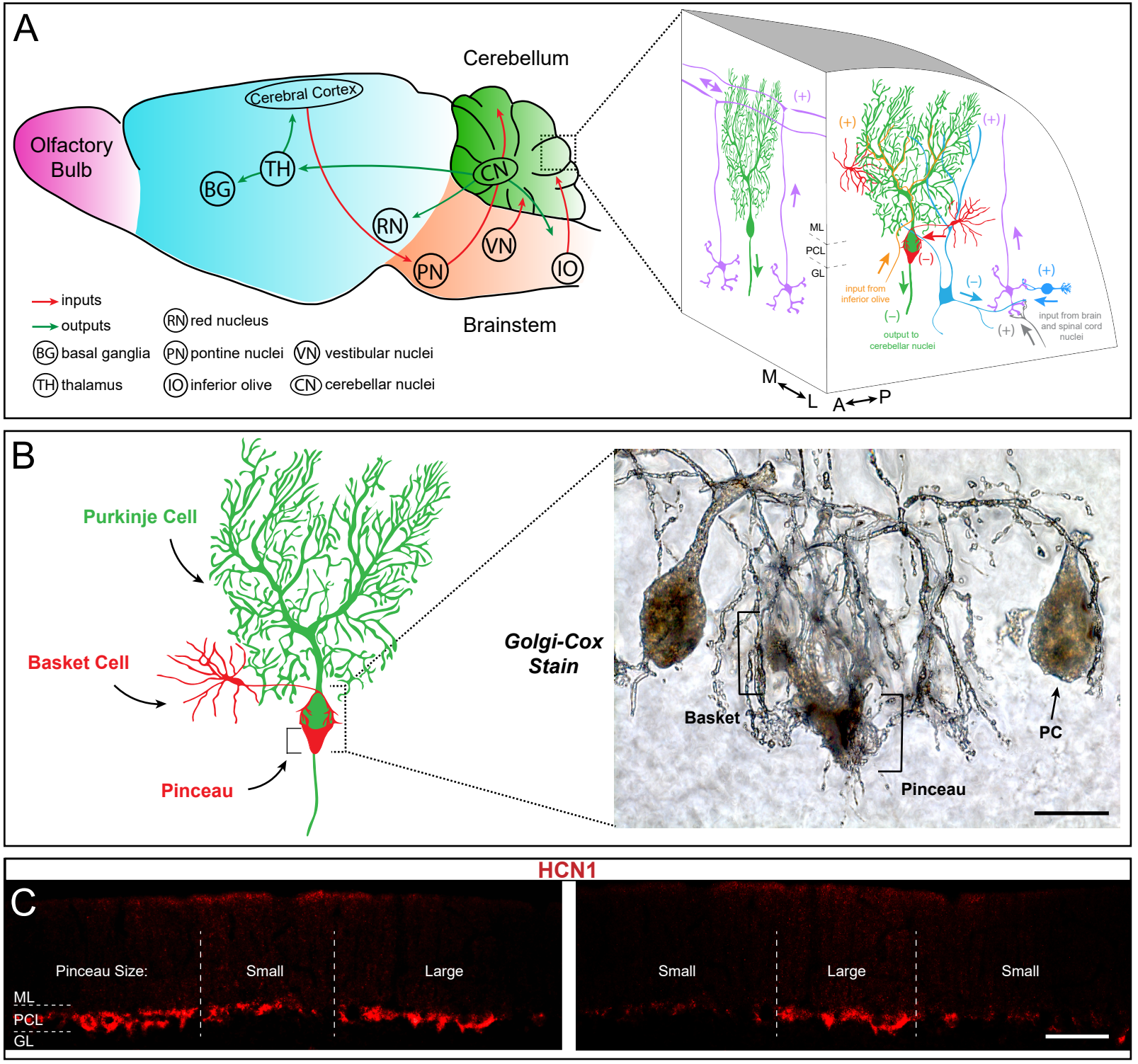
A
Cerebellum
Cerebral Cortex
Olfactory Bulb
TH
BG
CN
RN
PN
VN
IO
Brainstem
inputs
outputs
RN red nucleus
BG basal ganglia
PN pontine nuclei
VN vestibular nuclei
TH thalamus
IO inferior olive
CN cerebellar nuclei
(+)
(+)
(+)
ML
PCL
GL
input from inferior olive
(–)
(–)
output to cerebellar nuclei
(–)
(+)
(+)
input from brain and spinal cord nuclei
M
L
A
P
B
Purkinje Cell
Basket Cell
Pinceau
Golgi-Cox Stain
Basket
Pinceau
PC
HCN1
C
Pinceau Size:
Small
Large
Small
Large
Small
ML
PCL
GL

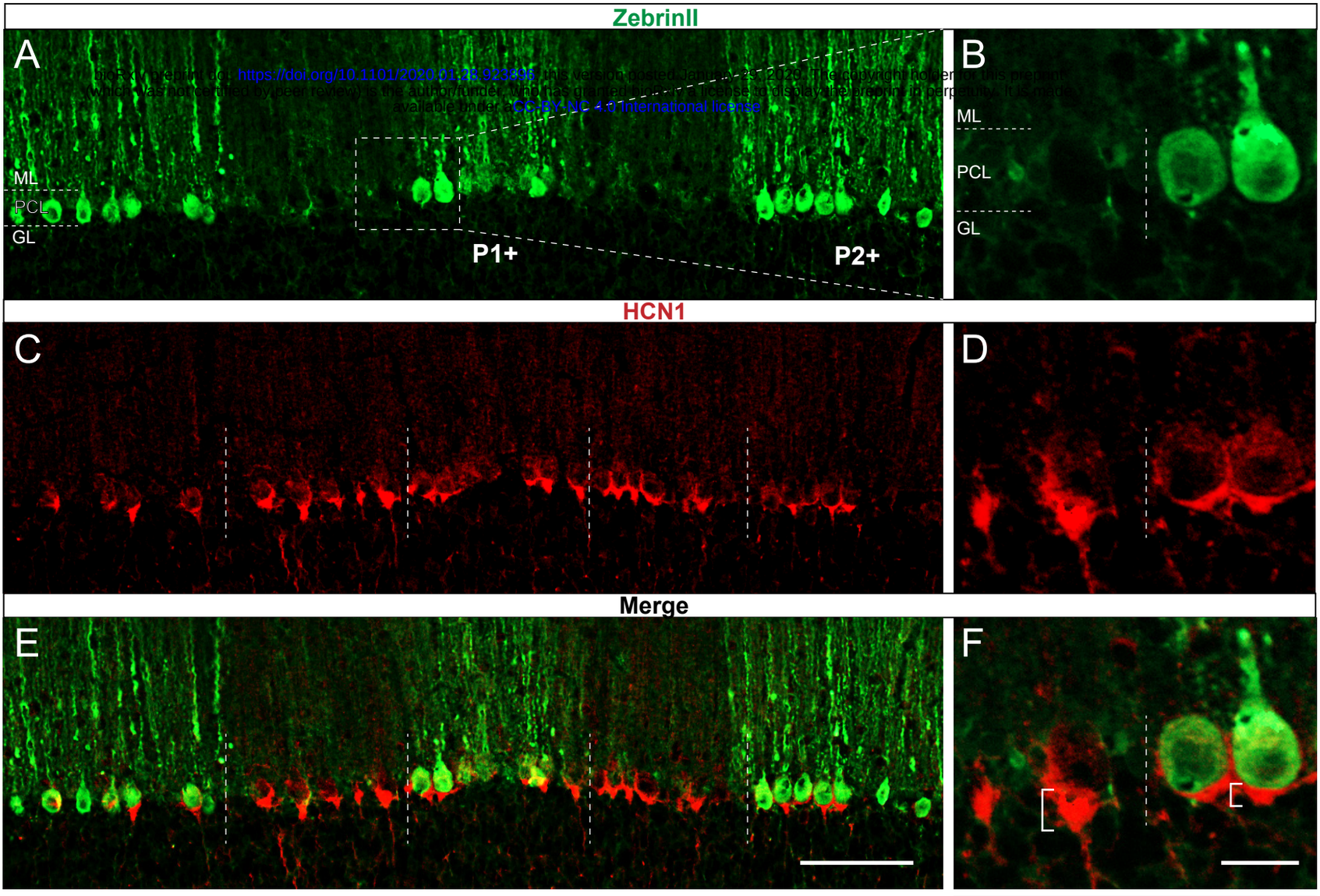

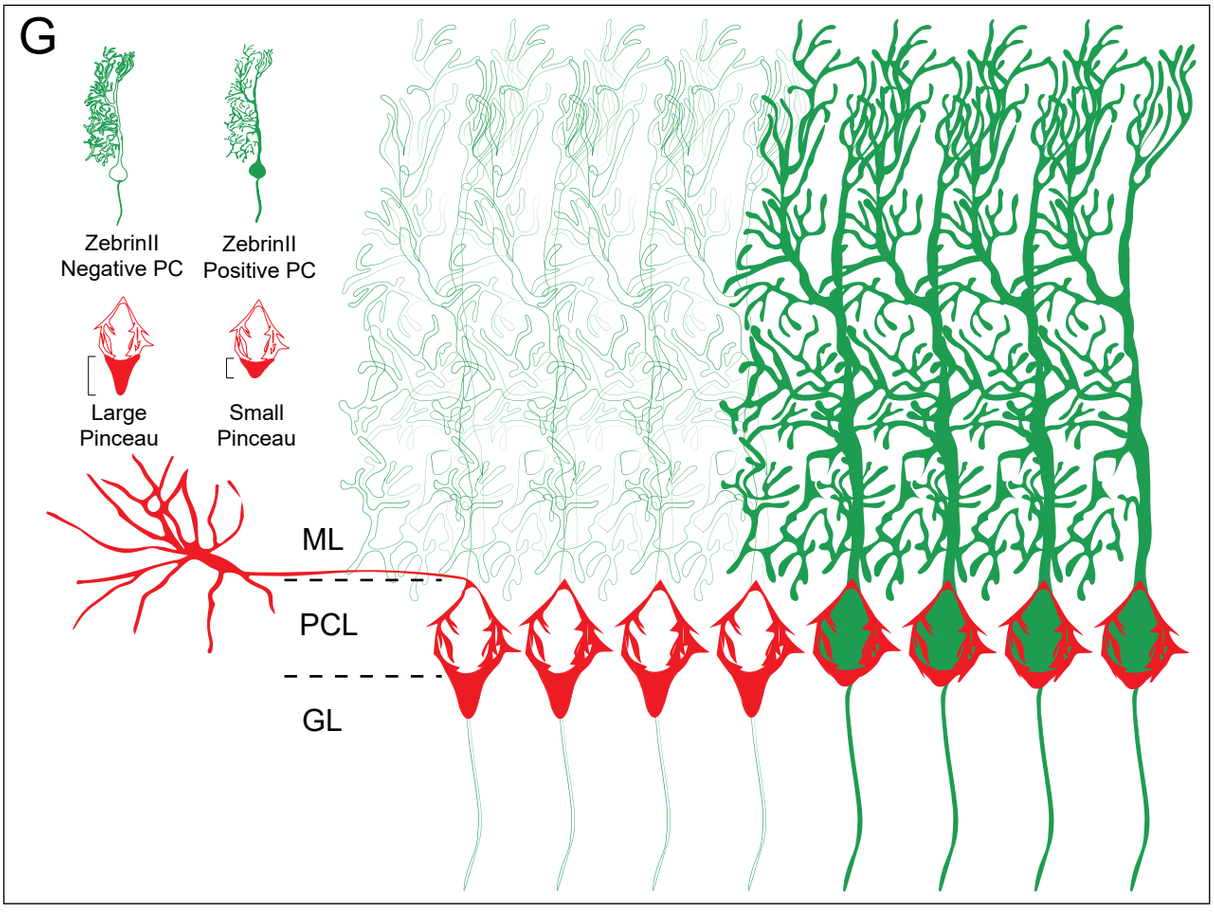

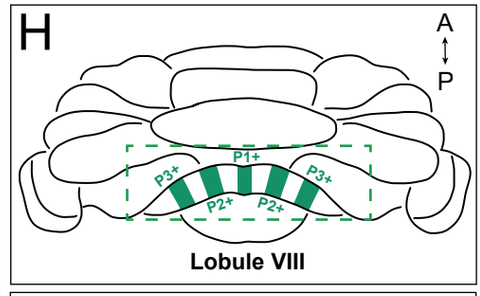

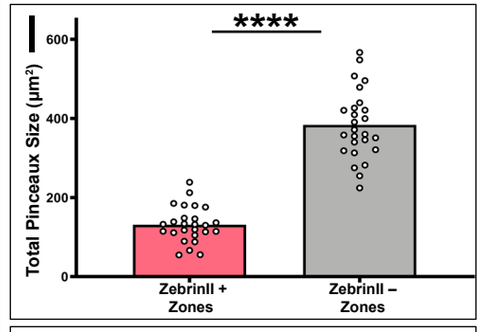

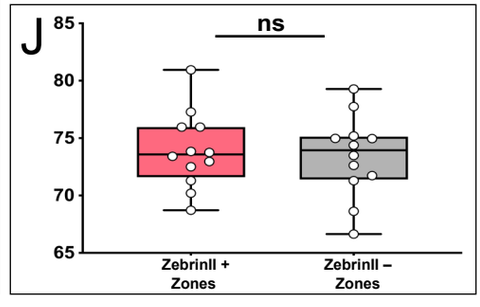

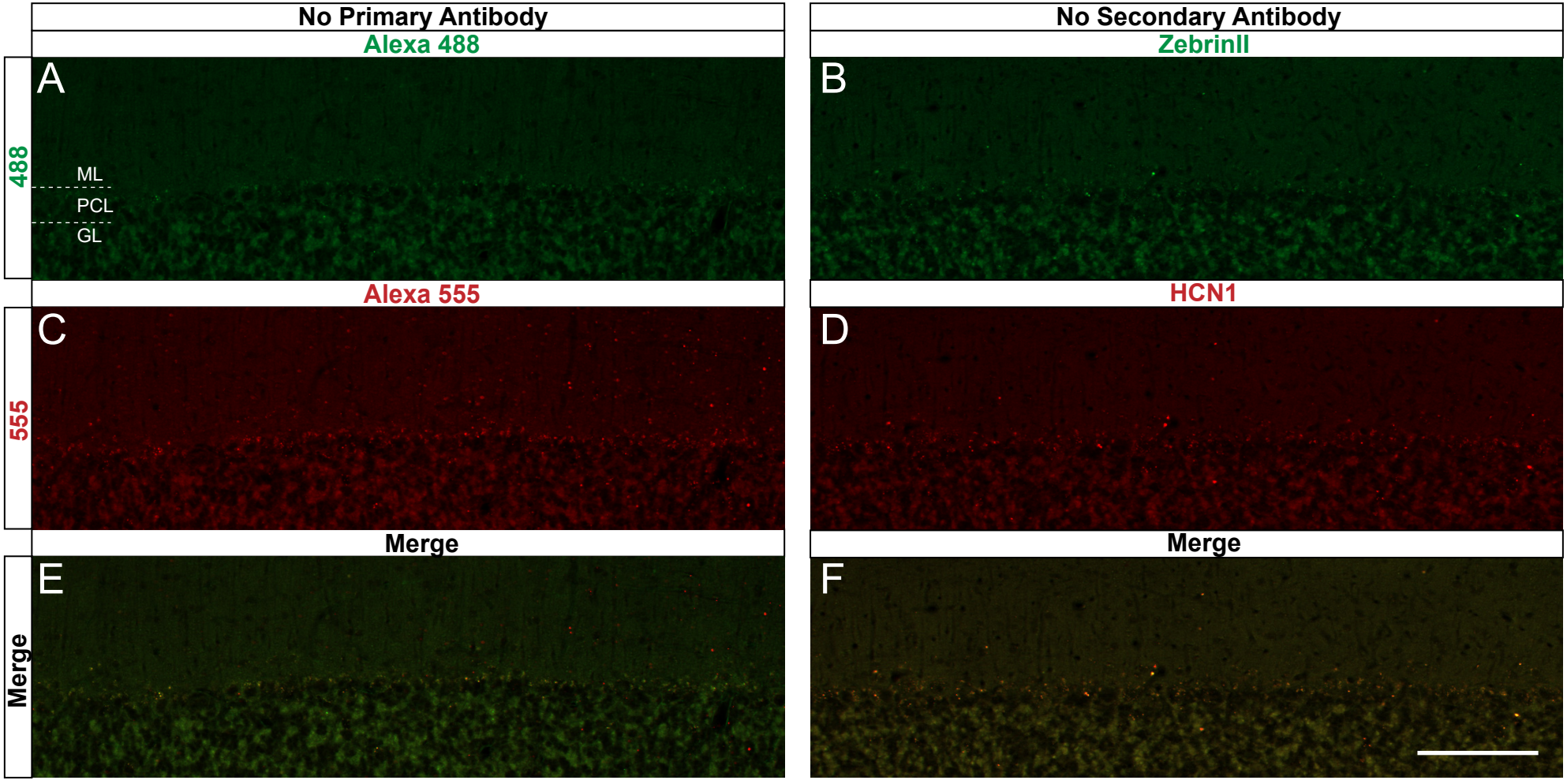
No Primary Antibody
Alexa 488
No Secondary Antibody
ZebrinII
A
B
488
ML
PCL
GL
Alexa 555
HCN1
C
D
555
Merge
Merge
E
F
Merge

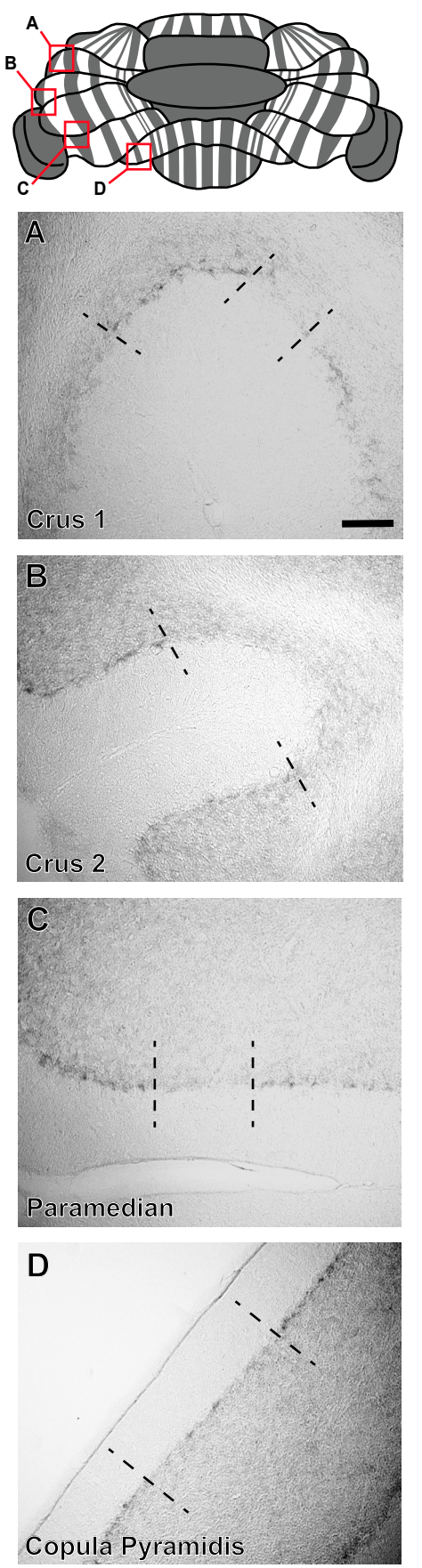
A
B
C
D
A
Crus 1
B
Crus 2
C
Paramedian
D
Copula Pyramidis

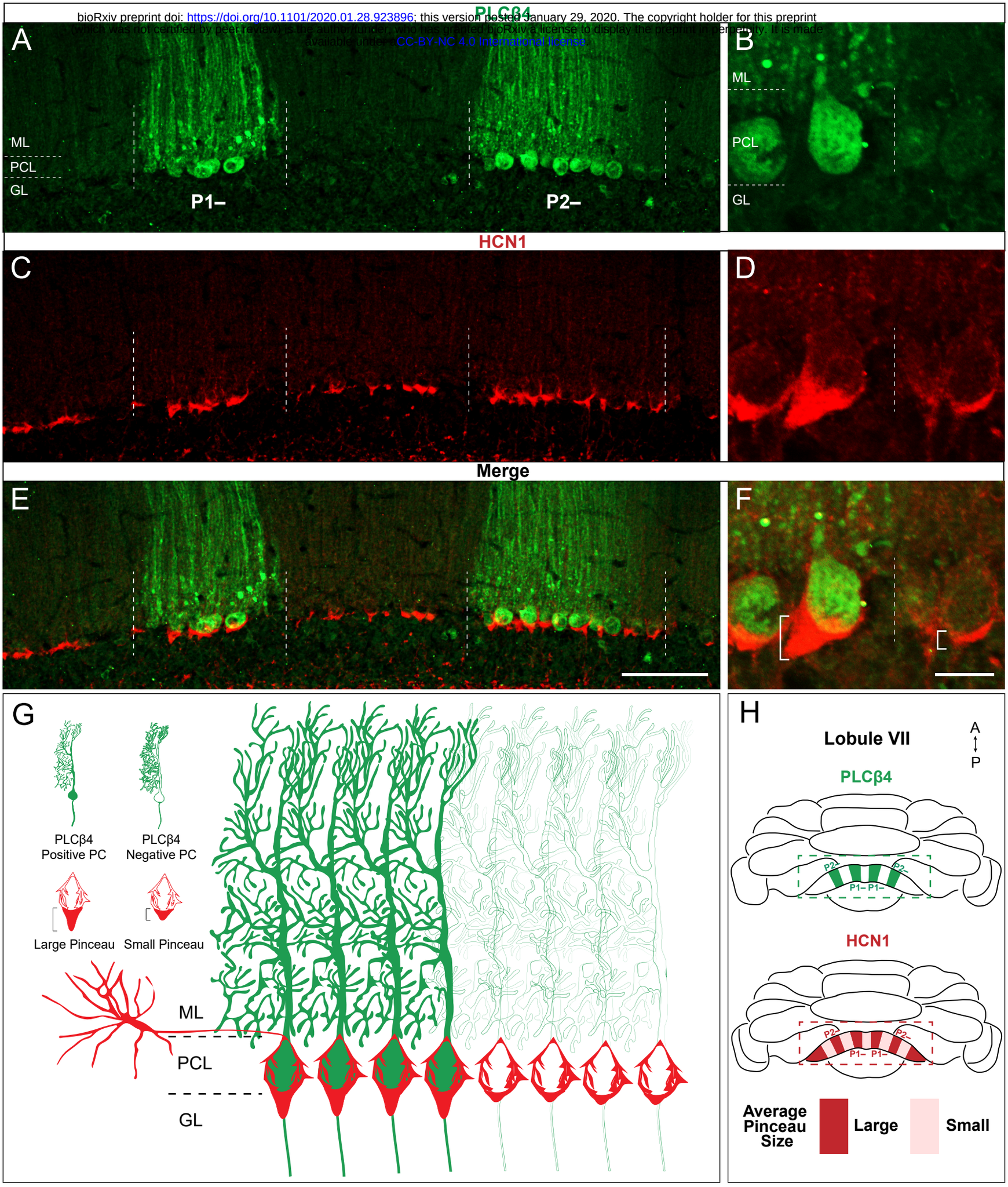

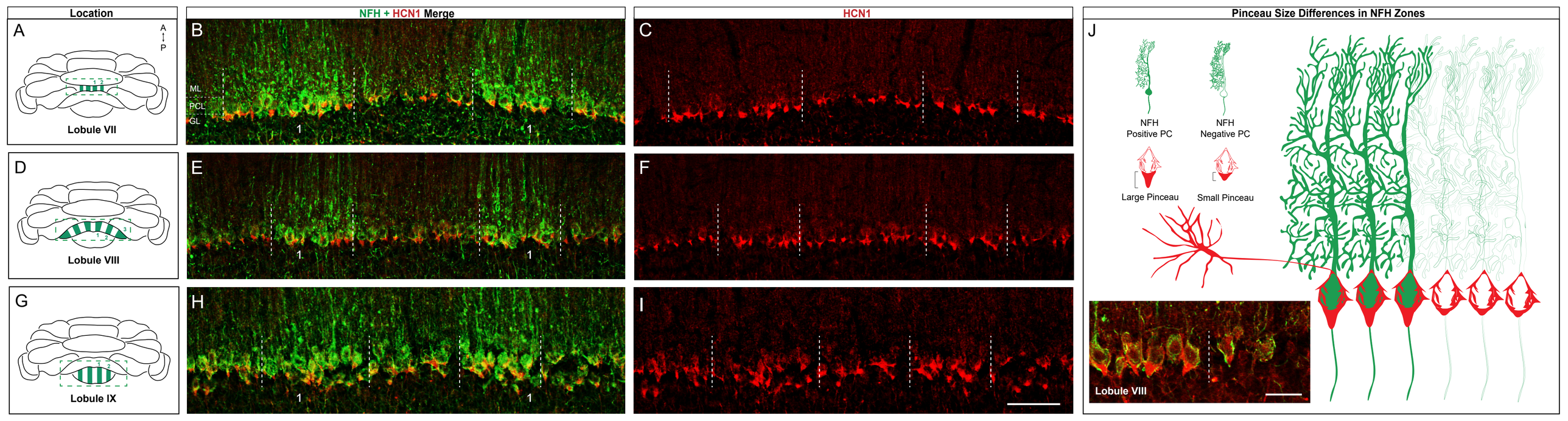
Location
A
A
P
Lobule VII
D
Lobule VIII
G
Lobule IX
NFH + HCN1 Merge
B
ML
PCL
GL
1
1
E
1
1
H
1
1
HCN1
C
F
I
Pinceau Size Differences in NFH Zones
J
NFH
Positive PC
NFH
Negative PC
Large Pinceau
Small Pinceau
Lobule VIII

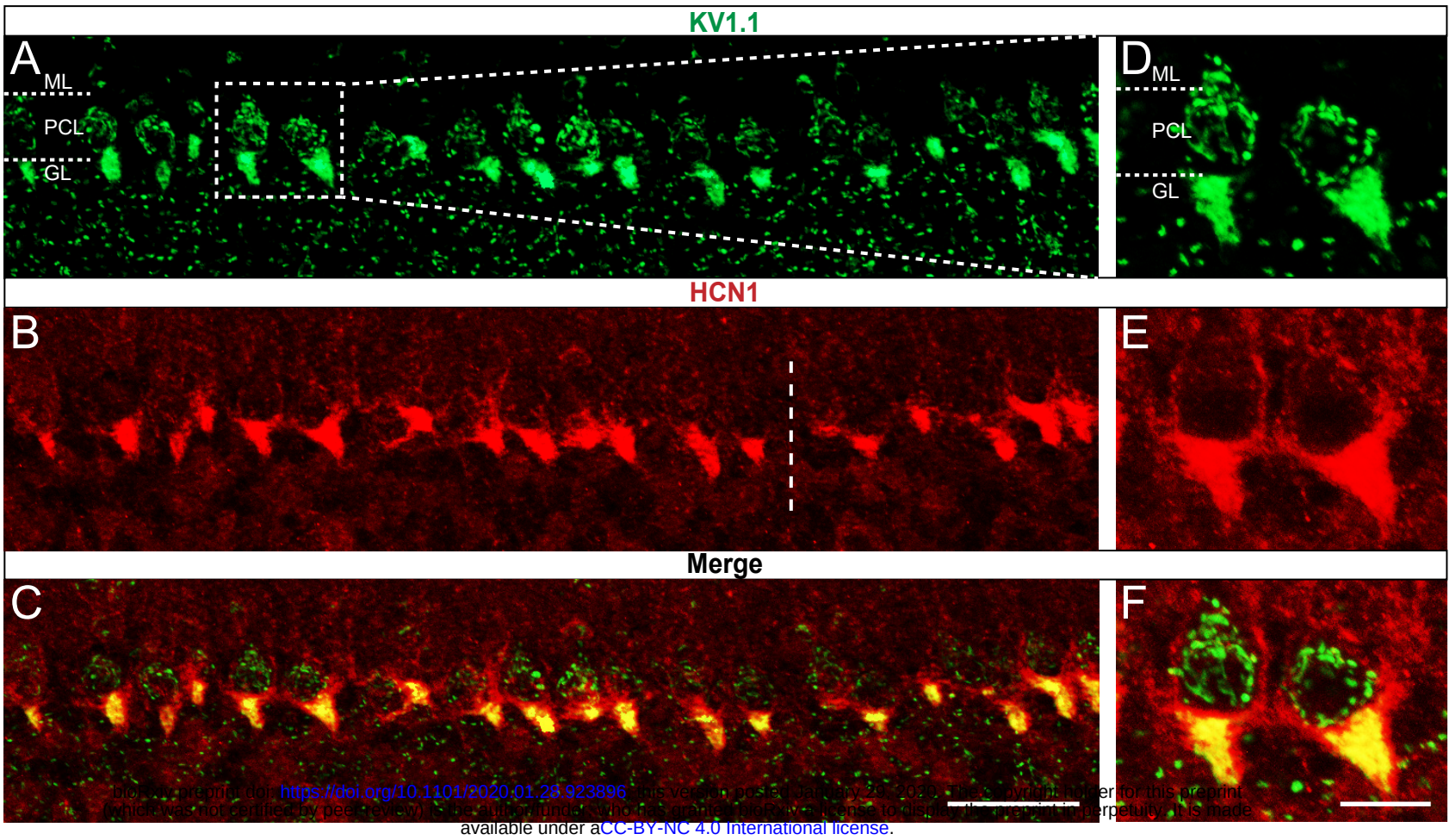

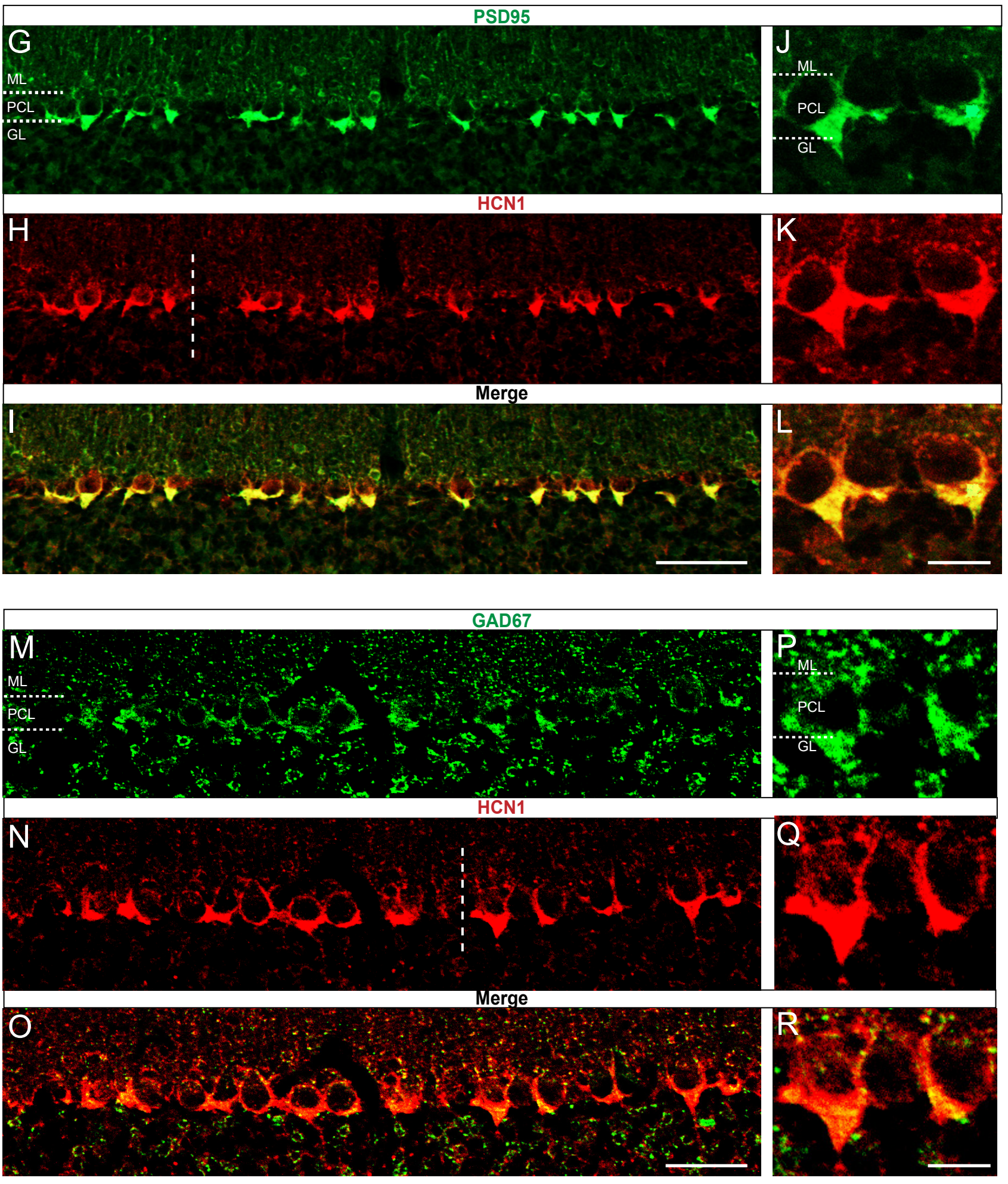

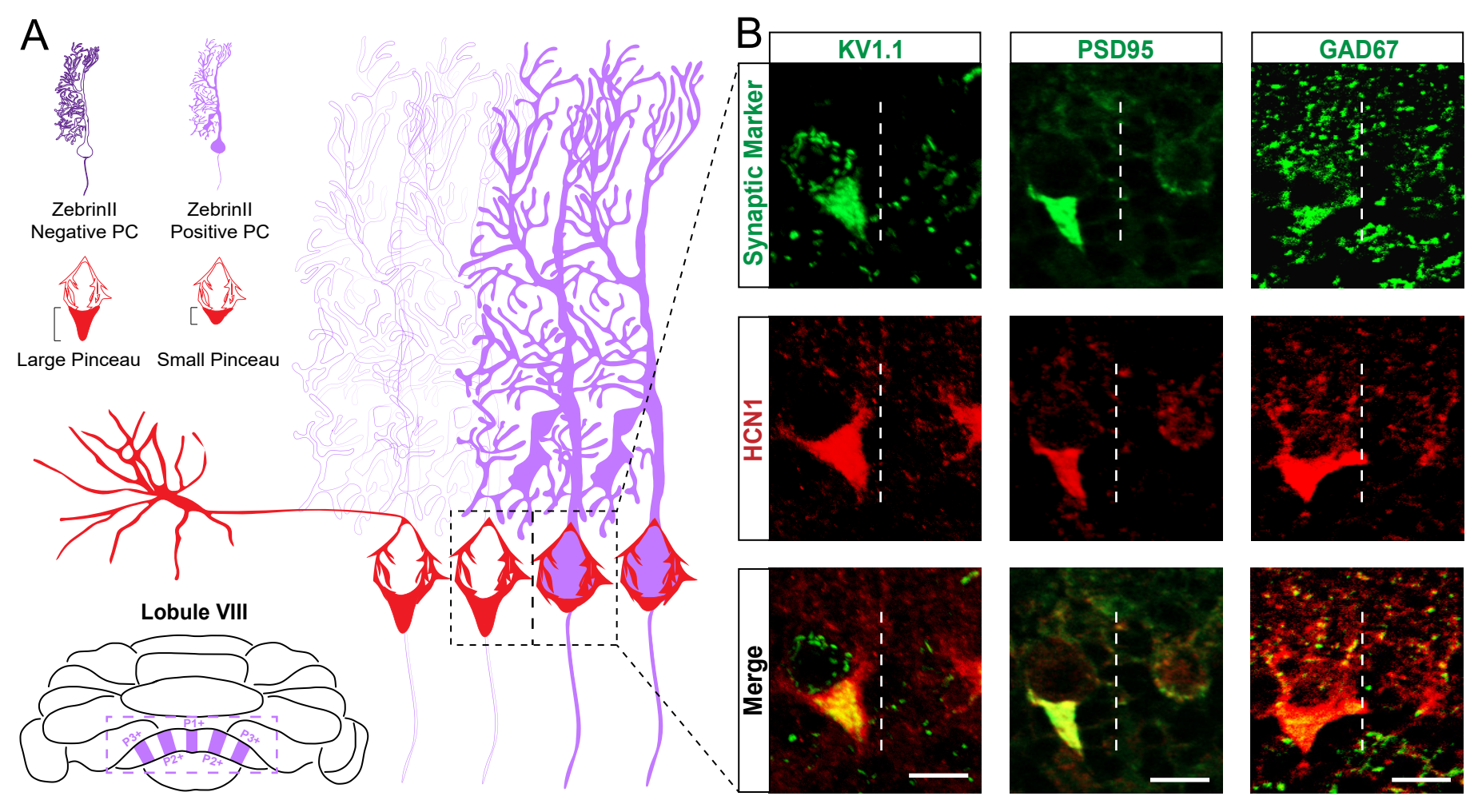
A
ZebrinII
Negative PC
ZebrinII
Positive PC
Large Pinceau
Small Pinceau
Lobule VIII
P1+
P2+
P2+
P3+
P3+
B
KV1.1
PSD95
GAD67
Synaptic Marker
HCN1
Merge

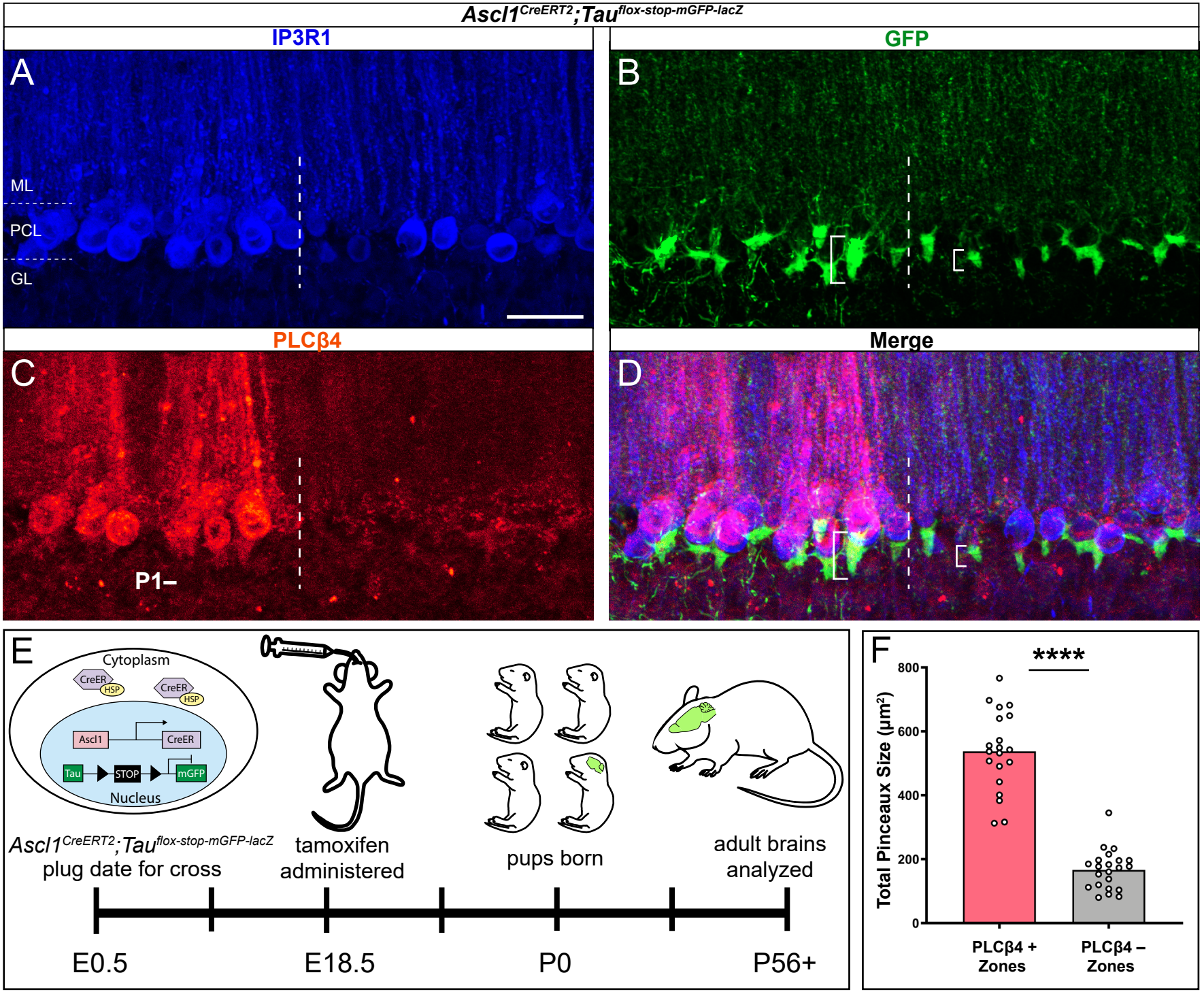
Ascl1CreERT2;Tauflox-stop-mGFP-lacZ
IP3R1
GFP
A
B
ML
PCL
GL
PLCβ4
Merge
C
D
P1–
E
Cytoplasm
CreER
HSP
CreER
HSP
Ascl1
CreER
Tau
STOP
mGFP
Nucleus
Ascl1CreERT2;Tauflox-stop-mGFP-lacZ
plug date for cross
tamoxifen
administered
pups born
adult brains
analyzed
E0.5
E18.5
P0
P56+
F
****
Total Pinceaux Size (µm²)
800
600
400
200
0
PLCβ4 +
Zones
PLCβ4 –
Zones

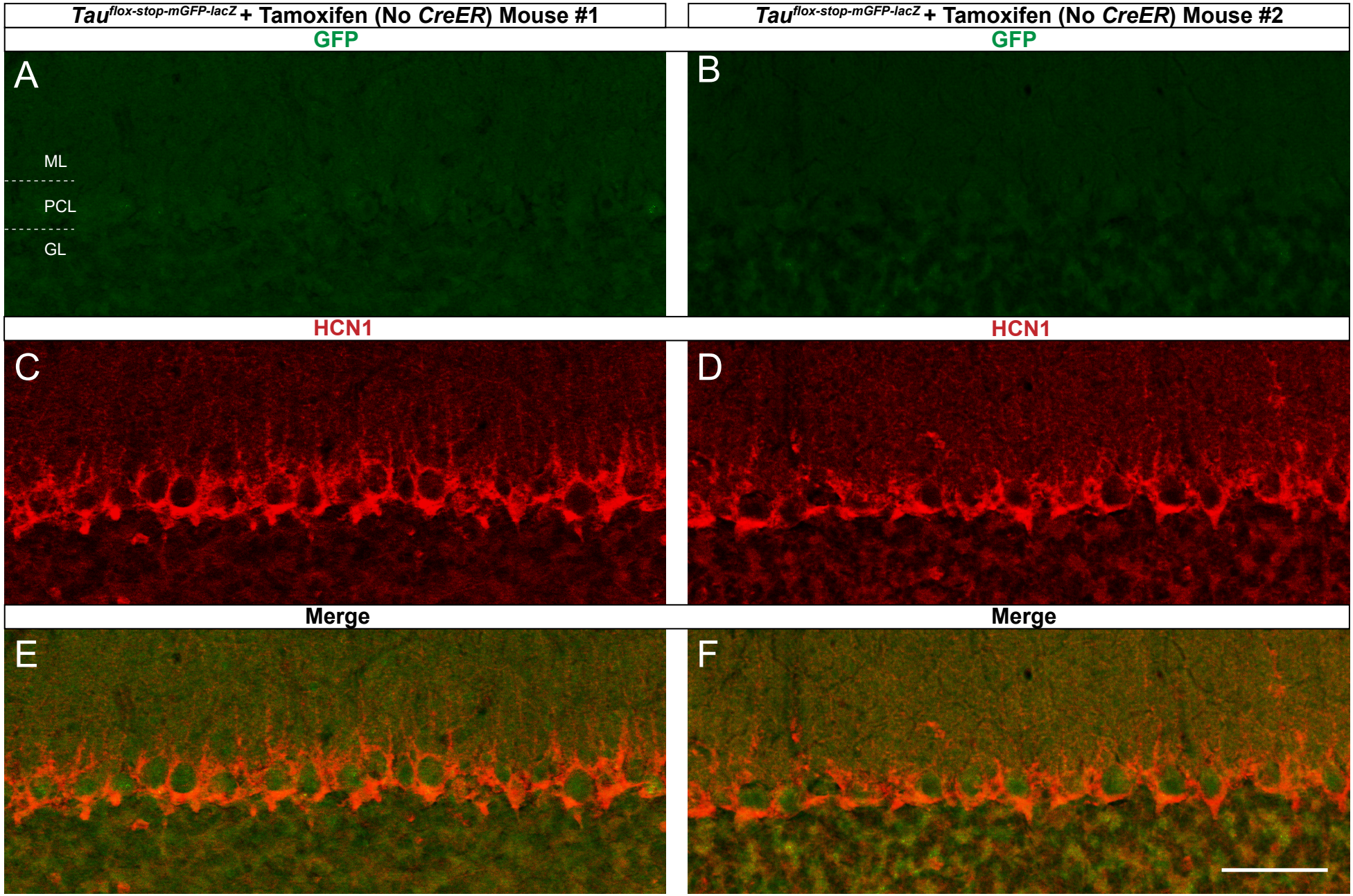
Tau flox-stop-mGFP-lacZ + Tamoxifen (No CreER) Mouse #1
Tau flox-stop-mGFP-lacZ + Tamoxifen (No CreER) Mouse #2
GFP
GFP
A
B
ML
PCL
GL
HCN1
HCN1
C
D
Merge
Merge
E
F

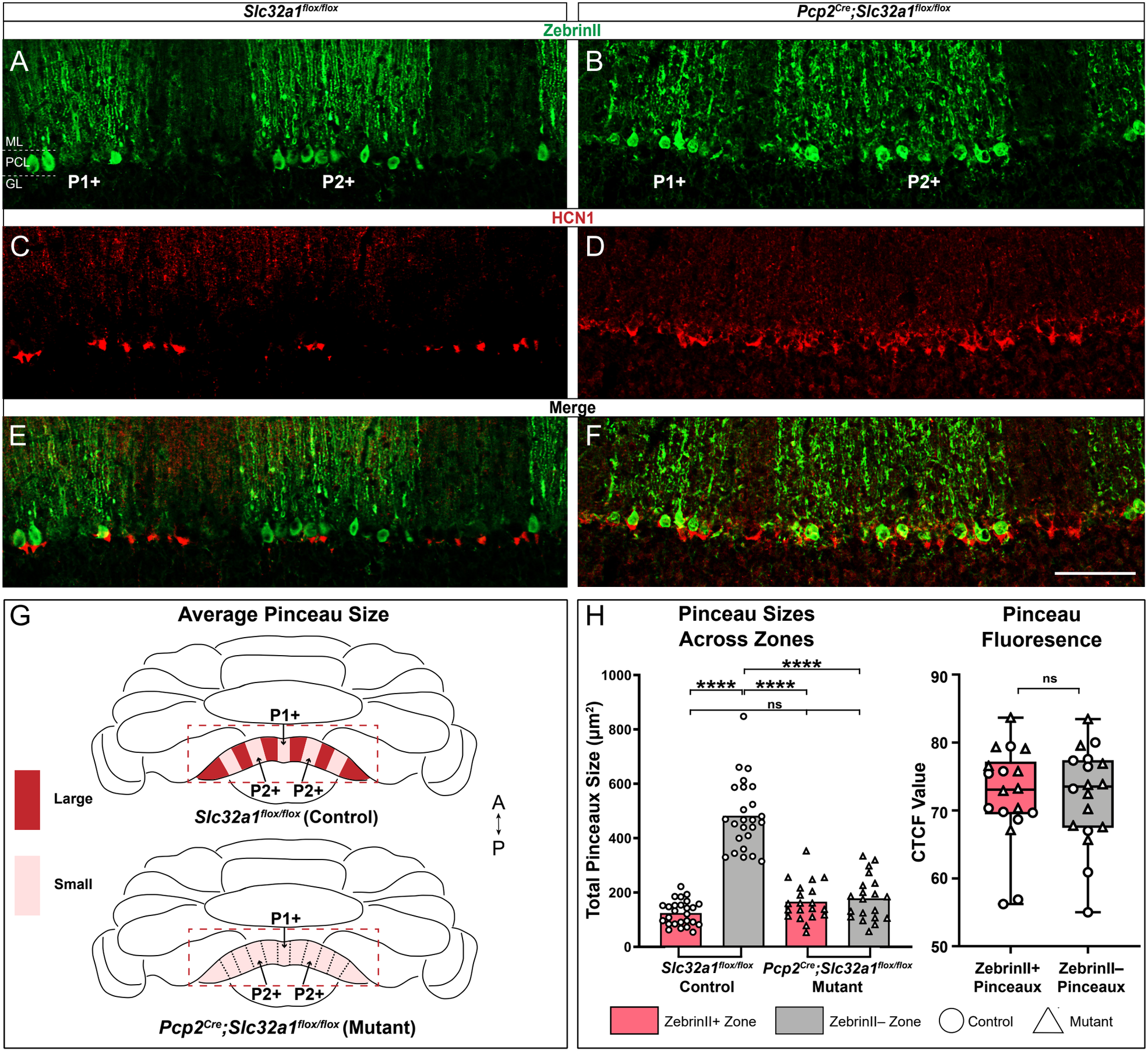
Slc32a1flox/flox
Pcp2Cre;Slc32a1flox/flox
ZebrinII
A
B
ML
PCL
GL
P1+
P2+
P1+
P2+
HCN1
C
D
Merge
E
F
G
Average Pinceau Size
P1+
P2+ P2+
Large
Small
Slc32a1flox/flox (Control)
A
P
P1+
P2+ P2+
Pcp2Cre;Slc32a1flox/flox (Mutant)
H
Pinceau Sizes Across Zones
Total Pinceaux Size (µm²)
1000
800
600
400
200
0
****
****
****
ns
Slc32a1flox/flox Control
Pcp2Cre;Slc32a1flox/flox Mutant
Pinceau Fluoresence
CTCF Value
90
80
70
60
50
ns
ZebrinII+ Pinceaux
ZebrinII– Pinceaux
ZebrinII+ Zone
ZebrinII– Zone
Control
Mutant

Whole Mount Zebrin Patterning

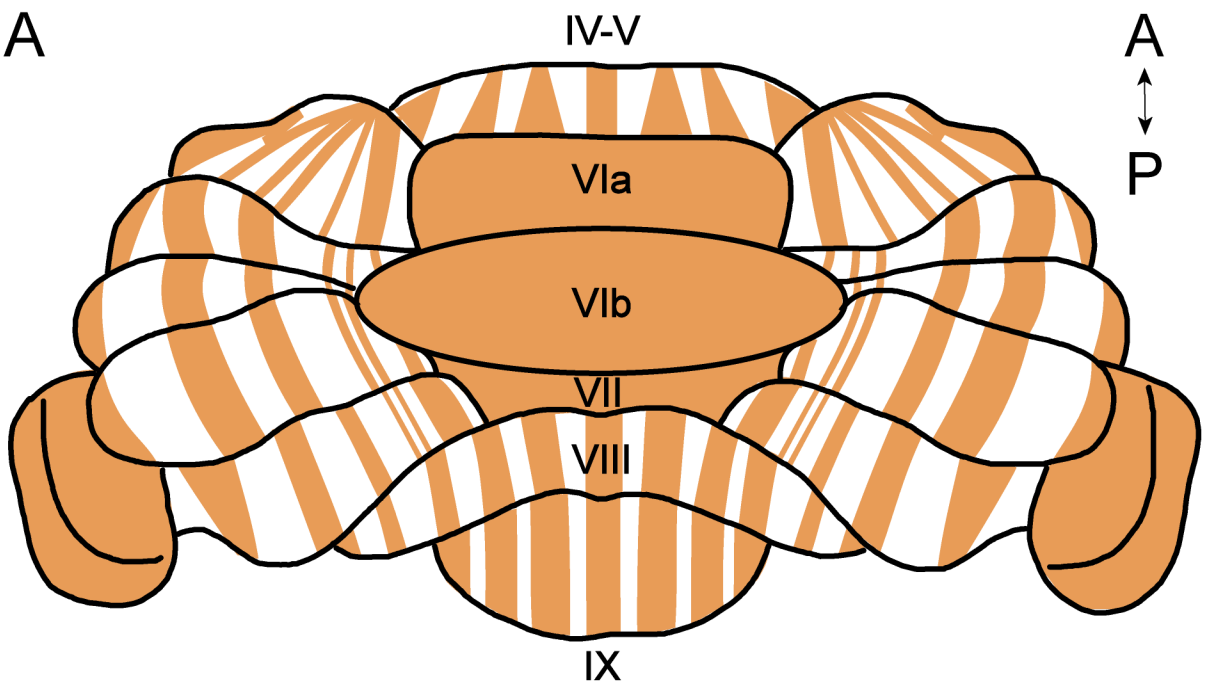

Sagittal Legend

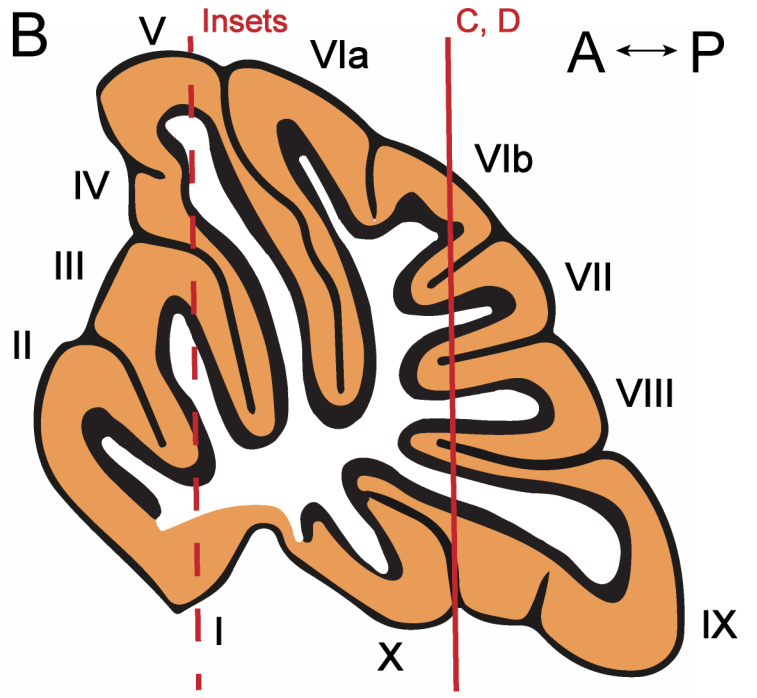

Slc32a1$^{flox/flox}$ (Control)

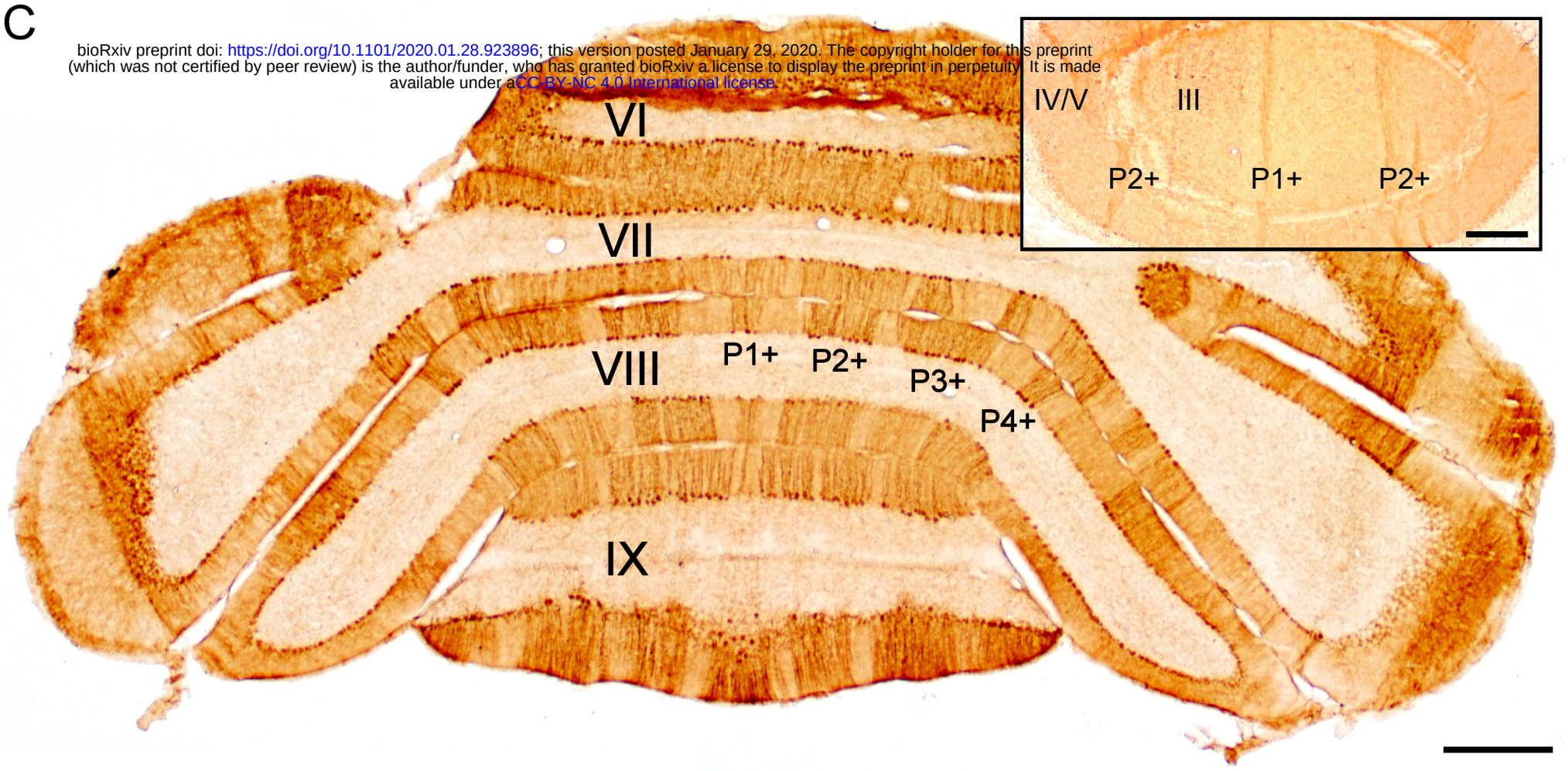

Ascl1^{CreERT2};*Slc32a1*$^{flox/flox}$ (Mutant)